Met Team Doc 96/9

SOUTHAMPTON OCEANOGRAPHY CENTRE

SOC INTERNAL DOCUMENT No.5

Air flow over the R.R.S. Charles Darwin: the disturbance of the flow at the anemometer sites used during cruises CD43 and CD98

B. I. Moat, M. J. Yelland

May 1996

Southampton Oceanography Centre
Empress Dock
Southampton
SO14 3ZH
Tele : (01703) 595000
Fax : (01703) 596400

ABSTRACT

The Computational Fluid Dynamics (CFD) package "Vectis" was used to model the effect of air flow distortion, caused by the hull and superstructure of the ship, on wind speed measurements made from two R.R.S. Charles Darwin cruises. Wind speed errors are calculated for the positions of the anemometers on CD43, which was instrumented with four fast sampling instruments used to measure the wind stress. This report describes the errors predicted by the model results: the comparison between model and cruise results is discussed in Yelland et al. (1996). Errors are also calculated for the anemometer positions on CD98 and CD98a, cruises where the ship carried an array of eleven anemometers for the purpose of evaluating the CFD package. The Vectis model considered in this report simulates a surface layer wind profile, directly over the bows of the ship, with a 10m wind speed of 13.8 m/s.

VECTIS REPORT NUMBER 3.1/14

AIR FLOW OVER THE R.R.S. CHARLES DARWIN: THE DISTURBANCE OF THE FLOW AT THE ANEMOMETER SITES USED DURING CRUISES CD43 AND 98

VECTIS REPORT NUMBER 3.1/14

AIR FLOW OVER THE R.R.S. CHARLES DARWIN: THE DISTURBANCE OF THE FLOW AT THE ANEMOMETER SITES USED DURING CRUISES CD43 AND CD98

B. I. Moat and M. J. Yelland
May 1996
Phase5 run time 10th January 1996 19th January 1996

1. Introduction

The Computational Fluid Dynamics (CFD) package "Vectis" was used to model the effect of air flow distortion, caused by the hull and superstructure of the ship, on wind speed measurements made during two R.R.S. Charles Darwin cruises. Wind speed errors are calculated for the positions of the anemometers on CD43, which was instrumented with four fast sampling instruments used to measure the wind stress. This report describes the errors predicted from the model: the comparison between model and cruise results is discussed in Yelland *et al.*, (1996). Errors are also calculated for the anemometer positions on CD98 and CD98a, cruises where the ship carried an array of eleven anemometers for the purpose of evaluating the CFD package. The comparison between the cruise and model results will be the subject of a separate paper.

The Vectis model run number 3.1/14 considered in this report simulates a surface layer wind profile, directly over the bows of the ship, with a 10m wind speed of 13.8 m/s. The profile was similar to that used for model run 1.6/13 of the Darwin (Hutchings, 1995; Moat and Yelland, 1995) which was performed using an earlier version of the Vectis software. Section 2 describes the wind tunnel dimensions and the monitoring points used to test for convergence. The surface geometry of the Darwin had been refined after the earlier run: details of the changes to the geometry are described in section 2. Section 3 describes the convergence of the model and the development of the profile. Data were extracted for the locations of the anemometers on cruises CD98 and CD98a (section 4). Section 5 compares the results from run 3.1/14 with runs 1.6/13 and 3.1/20, all of which simulate flow over the bows of the ship.

2. Description of model

2.1 Introduction

This section describes the dimensions of the ship and "wind tunnel" (the rectangular flow domain around the ship model), the logarithmic wind profile used (section 2.3) and the monitoring locations used to test for convergence of the model flow (section 2.4).

2.2 The wind tunnel dimensions

The tunnel used is the standard 0-degree tunnel of dimensions x = length (-300 to 300), y = height (0 to 150 m) and z = width (-150 to 150 m). The floor is specified as a wall boundary with roughness length $4.5*10^{-4}$ m. The sides and the roof of the tunnel are specified as zero gradient boundaries. The mesh file used is "goles.mesh4". The Femgen model has been modified and is located under:

/working/jrd/met1/archive/darwin/darwin_0deg/newlog1_3.1.14/darwin_files_3.1.14/DAR96.G20

The previous Femgen model, DARWIN.G20 (Figure 1a), represented the aerofoil above the monkey island as a rectangular block, whereas a more realistic geometry was used in the later model, DAR96.G20 (Figure 1b). Other alterations to the DARWIN.G20 model included: 1) accurate reproduction of the Immarsat dome above the bridge, 2) the CTD frame was changed from a block to an open frame, 3) The main mast was set to the correct height and 4) slight alterations were made to the dimensions of the bridge. The width of the foremast platform was increased by 0.22 m.

2.3 Wind profile used

The wind profile specified at the inlet of the tunnel is identical to the profile used in Vectis run 3.1/7 over the bows of the R.R.S. Discovery, which reproduces the profile abeam of the Charles Darwin foremast in Vectis run 1.6/13. The selection of this profile is discussed in Moat *et al.*, (1996).

2.4 Convergence

The velocity and pressure were monitored at six positions throughout the tunnel:

1) (-200, 20, 100) MON.0
2) (0, 20, 100) MON.1
3) (-200, 10, 100) MON.2
4) (0, 10, 100) MON.3
5) (200, 10, 100) MON.4
6) (33, 17, -1) MON.5

A graph of total velocity against time step is shown in Figure 2. A file containing all output variables was examined for the last 400 time steps. All variables had steadied to the third significant figure.

2.5 Conclusions

The run was shown to have converged, and a post processing file was written for the extraction of data.

3. Data extraction from phase6 of Vectis

3.1 Introduction

A post processing file was written at time step 84 seconds, after more than 1900 iterations. The free stream velocity abeam of the ship (section 3.2) and the shape of the wind profile (section 3.3) were examined.

3.2 Checks on the free stream velocity

Lines of horizontal velocity data were extracted along the tunnel at ($-250 \leq x \leq 250$, $y=10$, $z=100$), ($-250 \leq x \leq 250$, $y=30$, $z=100$), ($-250 \leq x \leq 250$, $y=30$, $z=100$) and ($-250 \leq x \leq 250$, $y=50$, $z=100$), as shown in Figure 3a. This is reproduced in greater detail in Figure 3b, giving velocity data at ($-50 \leq x \leq 50$, $y=10:50$, $z=100$) i.e. directly abeam of the ship. The difference between velocity at the inlet and outlet is -0.034 m/s at a height of 10m, 0.001 m/s at a height of 20m, 0.099 m/s at a height of 30m and 0.042 m/s at a height of 50m, which indicates a very small change down the tunnel. These results show that free stream exists on a plane at z=100m, i.e. that the ship is not causing a significant blockage to the flow through the tunnel.

3.3 Checks on the wind profile

Profile data were extracted at a free stream plane close to the inlet ($x=250$, $0 \leq y \leq 150$, $z=100$) and close to the outlet ($x=-250$, $0 \leq y \leq 150$, $z=100$) and are shown in Figure 4. Figure 5 shows the difference between these inlet and outlet profiles. There is a maximum difference of -0.7 m/s at a height of 1 m, but over most heights the difference is less than 0.1 m/s which indicates that the profile changes very little along the tunnel.

3.4 Conclusions

Checks on the free stream velocity, 100m abeam of the ship at heights of y=10 m, y=20m, y=30m and y=50m, showed that a free stream velocity plane exists and that the ship was not blocking the air flow in the tunnel. Free stream velocities abeam of the anemometer positions were used to calculate velocity errors at the anemometer sites. The wind profile does not degrade significantly along the tunnel.

4. Charles Darwin CD98 and CD98a "GOLES" cruises

4.1 Introduction

This section examines the error in the wind speed measurements made from a number of anemometers mounted on Charles Darwin CD98 "GOLES" passage leg and the following Trials cruise CD98a. The run is at 0 degrees to the wind profile, i.e. the ship is "head to wind". The locations of the anemometer sites are, in the Vectis model co-ordinate system:

Research sonic (port side of foremast)	(20.319, 15.2, -2.55)
Wind master sonic(stb. side of foremast)	(30.218, 15.5, 2.86)
Young AQ (port side of foremast)	(30.918, 15.75, -1.0)
Young AQ (stb. side of foremast)	(30.918, 15.7, 2.0)
Vector 1 (port side of monkey island)	(15.56, 19.15, -1.725)
Vector 2 (port side of monkey island)	(15.56, 17.15, -1.725)
Vector 3 (port side of monkey island)	(15.56, 15.65, -1.725)
Vector 4 (port side of monkey island)	(15.56, 18.18, -1.725)
Vector 5 (port side of monkey island)	(15.56, 16.38, -1.725)
Wind master sonic (port side of main mast)	(-6.9, 25.15, -1.0)
Young (port side of main mast)	(-6.9, 24.70, -2.0)

The positions of the foremast anemometers are indicated in Figure 6, whilst the anemometers located above the monkey island are shown in Figure 7. It is worth noting that the Vector instruments, in order of height, are Vector 3 (lowest), Vector 5, Vector 2, Vector 4 and Vector 1 (highest).

4.2 Vertical displacement of the airflow

For a full description of the method used to calculate the vertical displacement of the air and the free stream height, refer to Moat *et al.*, (1996).

The vertical planes (K planes) may not coincide exactly with the plane of cells containing the anemometer. The centre plane of the model is K23. K19 is closest to the Research Sonic mounted on the port side of the foremast platform.

K18	z=-3.4685 m	
K19	z=-2.5806 m	Research Sonic at z=-2.55 m
K20	z=-1.7234 m	

For the Research sonic anemometer, the air flow has been raised by 1.187 m from it's original height before it reaches the anemometer location (Table 1).

Location	x (m)	y (m)	z (m)
Research sonic	30.218	15.2	-2.55
Z_{anemom}	30.242	15.255	-2.5809
sonic-Z_{anemom}	-0.024	-0.02	0.0309
Z_{origin}	164.95	14.068	-2.5809
Z_{anemom}-Z_{origin}	-134.708	**1.187**	0

Table 1 Vertical displacement of the air flow at the Research sonic anemometer site.

For the Wind Master sonic mounted on the starboard side of the foremast, the local planes are :

K25 z=2.564 m Wind Master sonic at z=2.86 m

K26 z=3.450 m

For the Wind master sonic anemometer the air flow has been raised by 1.188 m from it's original height before it reaches the anemometer location (Table 2).

Wind master sonic	30.218	15.5	2.86
Z_{anemom}	30.201	15.546	2.5638
sonic-Z_{anemom}	0.017	-0.046	0.2962
Z_{origin}	167.06	14.358	2.5638
Z_{anemom}-Z_{origin}	-136.859	**1.188**	0

Table 2 Vertical displacement of the air flow at the Wind Master sonic anemometer site.

For the Young AQ mounted on the port side of the foremast, the local planes are :

K20 z=-1.723 m

K21 z=-0.866 m Young AQ at z=-1.0 m

For the Young AQ anemometer the air flow has been raised by 1.24 m from it's original height before it reaches the anemometer location (Table 3).

Young AQ	30.918	15.7	-1
Z_{anemom}	30.940	15.678	-0.866
Young-Z_{anemom}	-0.022	0.022	-0.134
Z_{origin}	190.54	14.438	-0.866
Z_{anemom}-Z_{origin}	-159.6	**1.24**	0

Table 3 Vertical displacement of the air flow at the port Young AQ anemometer site.

For the Young AQ mounted on the starboard side of the foremast, the local planes are :

K24 z=1.706 m Young AQ at z=2.0 m

K25 z=2.564 m

For the Young AQ anemometer the air flow has been raised by 1.169 m from it's original height before it reaches the anemometer location (Table 4).

Young AQ	30.918	15.75	2.0
Z_{anemom}	30.950	15.741	1.7064
Young-Z_{anemom}	-0.032	0.009	0.2936
Z_{origin}	166.26	14.572	1.706
Z_{anemom}-Z_{origin}	-135.31	**1.169**	0

Table 4 Vertical displacement of the air flow at the starboard Young AQ anemometer site.

For the Vector anemometers mounted above the Monkey island, the local planes are :

K19 z=-2.5806 m

K20 z=-1.7234 m All Vector anemometers at z=-1.725 m.

The displacements for the Vector instruments are shown in Table 5 and are summarised in Table 6.

Vector 1	15.56	19.15	-1.725
Z_{anemom}	15.680	19.21	-1.7234
Vector1-Z_{anemom}	-0.12	-0.06	-0.0016
Z_{origin}	190.27	16.33	-1.7234
Z_{anemom}-Z_{origin}	-174.59	**2.88**	0
Vector 2	15.56	17.15	-1.725
Z_{anemom}	15.606	17.154	-1.7234
Vector2-Z_{anemom}	-0.046	-0.004	-0.0016
Z_{origin}	166.80	14.067	-1.7234
Z_{anemom}-Z_{origin}	-151.194	**3.087**	0
Vector 3	15.56	15.65	-1.725
Z_{anemom}	15.543	15.70	-1.7234
Vector3-Z_{anemom}	0.017	-0.05	-0.0016
Z_{origin}	166.65	9.5458	-1.7234
Z_{anemom}-Z_{origin}	-151.107	**6.1542**	0
Vector 4	15.56	18.18	-1.725
Z_{anemom}	15.5535	18.235	-1.7234
Vector4-Z_{anemom}	0.0065	-0.055	-0.0016
Z_{origin}	164.84	15.179	-1.7234
Z_{anemom}-Z_{origin}	-149.29	**3.056**	0
Vector 5	15.56	16.38	-1.725
Z_{anemom}	15.559	16.352	-1.7234
Vector5-Z_{anemom}	0.001	0.028	-0.0016
Z_{origin}	191.11	13.311	-1.7234
Z_{anemom}-Z_{origin}	-175.55	**3.041**	0

Table 5 Vertical displacement of the air flow at the Vector anemometer sites.

Vector	3 (lowest)	5	2	4	1 (highest)
Displacement (m)	6.154	3.041	3.087	3.056	2.88

Table 6. Vertical displacement of the air flow at the Vector anemometer sites, in order of instrument height.

For the Wind master sonic mounted on the port side of the main mast, the local planes are :

K20 z=-1.7234 m

K21 z=-0.866 m Wind master sonic at z=-1.0 m

For the Wind master sonic anemometer the air flow has been raised by 2.18 m from it's original height before it reaches the anemometer location (Table 7)

Wind master sonic	-6.9	25.15	-1.0
Z_{anemom}	-6.9228	25.135	-0.866
sonic-Z_{anemom}	0.0228	0.015	-0.134
Z_{origin}	189.94	22.959	-0.866
Z_{anemom}-Z_{origin}	-196.86	**2.176**	0

Table 7 Table showing the amount the air is raised when it reaches the Windmaster sonic anemometer site.

For the Young AQ mounted on the port side of the main mast, the local planes are :

K19 z=-2.5806 m

K20 z=-1.7234 m Young AQ at z=-2.0 m

K21 z=-0.866 m

For the Young AQ anemometer the air flow has been raised by 2.15 m from it's original height before it reaches the anemometer location (Table 8)

Young AQ	-6.9	24.70	-2.0
Z_{anemom}	-6.9558	24.798	-1.7234
sonic-Z_{anemom}	0.0558	-0.098	-0.2766
Z_{origin}	161.63	22.640	-1.7234
Z_{anemom}-Z_{origin}	-168.59	**2.152**	0

Table 8 Table showing the amount the air is raised when it reaches the Wind master sonic anemometer site.

4.3 Free stream velocities

A value of the wind speed in free stream conditions is needed in order to obtain a wind speed error at the anemometer site. The free stream site used is that towards the edge of the tunnel directly abeam of the anemometer site. The free stream velocity is taken from the

profile at the height at which the air originated, i.e. the anemometer height minus the amount the air has been raised (Moat *et al.*, 1996). Free stream velocities, taken from the free stream plane, directly abeam of the anemometer sites are shown in Table 9.

Anemometer	Free stream velocity (m/s)	Height free stream velocity originated from (m)
Research sonic (port)	**14.077**	14.103
Windmaster sonic (stb.)	**14.097**	14.312
Young AQ (port)	**14.106**	14.460
Young AQ (stb.)	**14.115**	14.581
Vector 1	**14.299**	16.270
Vector 2	**14.089**	14.063
Vector 3	**13.718**	9.496
Vector 4	**14.162**	15.179
Vector 5	**14.039**	13.339
Windmaster sonic (port main mast)	**14.583**	22.974
Young AQ (port main mast)	**14.563**	22.548

Table 9 Table showing the free stream velocities for each anemometer.

4.4 Velocities at anemometer locations

For the method of extracting data refer to Moat *et al.* (1996).

The percentage wind speed error is given by:

$$\text{error} = \left(\frac{\text{Average Velocity}}{\text{Free stream velocity}} - 1 \right) * 100 \qquad (1)$$

Figures 8 to 18 show the lines of data through the Research sonic (port foremast), Wind master sonic (starboard foremast) Young AQ (port foremast), Young AQ (starboard foremast), Vector 1, Vector 2, Vector3, Vector 4, Vector 5, Windmaster sonic (port mainmast) and Young AQ (port mainmast) respectively.

The results for all anemometers are summarised in Table 10, which also includes the values that the air flow has been displaced vertically.

Anemometer	Velocity from each direction (m/s)	Average velocity (m/s)	Free stream velocity (m/s)	wind speed error (%)	vertical displacement (m)
Research sonic Port foremast	13.591 (x)				
	13.595 (y)	13.594	14.077	**-3.431**	**1.187**
	13.597 (z)				
Wind master sonic Stb. foremast	13.629 (x)				
	13.632 (y)	13.630	14.097	**-3.315**	**1.188**
	13.628 (z)				
Young AQ port foremast	13.005 (x)				
	12.958 (y)	12.996	14.106	**-7.869**	**1.240**
	13.025 (z)				
Young AQ Stb. foremast	13.407 (x)				
	13.396 (y)	13.401	14.115	**-5.061**	**1.169**
	13.399 (z)				
Vector 1	15.017 (x)				
	14.957 (y)	14.986	14.229	**5.323**	**2.88**
	14.985 (z)				
Vector 2	13.255 (x)				
	13.252 (y)	13.254	14.089	**-5.930**	**3.087**
	13.110 (z)				
Vector 3	13.996 (x)				
	13.816 (y)	13.959	13.718	**1.757**	**6.154**
	13.922 (z)				
Vector 4	14.444 (x)				
	14.312 (y)	14.162	14.445	**1.995**	**3.056**
	14.445 (z)				
Vector 5	13.520 (x)				
	13.594 (y)	13.518	14.039	**-3.711**	**3.041**
	13.440 (z)				
Wind master sonic Port main mast	15.069 (x)				
	15.071 (y)	15.070	14.583	**3.340**	**2.176**
	15.070 (z)				
Young AQ Port main mast	15.053 (x)				
	15.045 (y)	15.050	14.563	**3.344**	**2.152**
	15.052 (z)				

Table 10 Error estimates at the anemometer sites on CD98 and CD98a.

4.5 Rates of change at the anemometer sites

This section examines the rate of change of velocity around the anemometer site using Figures 8 to 18. This gives an indication of the accuracy of the wind speed errors and of the suitability of the location for obtaining reliable wind speed measurements. The rate of change of velocity is given in terms of change per cell and per meter in Table 11.

Anemometer	Velocity data line	Rate of change of velocity per meter (ms^{-1}/m)	Rate of change of velocity per cell (ms^{-1}/cell)
Research sonic Port foremast	along (x)	0.200	0.0292
	up (y)	0.080	0.0027
	across (z)	0.011	0.0092
Wind master sonic Stb. foremast	along (x)	0.1275	0.0181
	up (y)	0.0225	0.0029
	across (z)	0.0360	0.0123
Young AQ port foremast	along (x)	0.518	0.0934
	up (y)	0.350	0.122
	across (z)	1.549	0.188
Young AQ Stb. foremast	along (x)	0.124	0.0360
	up (y)	0.228	0.0712
	across (z)	0.260	0.0426
Vector 1	along (x)	0.0805	0.0260
	up (y)	0.393	0.161
	across (z)	0.342	0.362
Vector 2	along (x)	0.016	0.0649
	up (y)	0.208	0.0891
	across (z)	1.192	0.318
Vector 3	along (x)	0.140	0.106
	up (y)	3.599	0.127
	across (z)	0.461	0.164
Vector 4	along (x)	0.095	0.0352
	up (y)	0.850	0.500
	across (z)	1.117	0.242
Vector 5	along (x)	0.397	0.140
	up (y)	0.045	0.286
	across (z)	0.650	0.188
Wind master sonic Port main mast	along (x)	0.0115	0.00505
	up (y)	0.009	0.00275
	across (z)	0.0115	0.00285
Young AQ Port main mast	along (x)	0.013	0.0170
	up (y)	0.026	0.0441
	across (z)	0.012	0.0314

Table 11 Rate of change of velocity close to the anemometer sites

The rate of change of velocity per meter is large for the Research and Windmaster sonic anemometers on the foremast platform. Compared to the sonics, the Young AQ anemometer positions are relatively close to the foremast extension and hence the rates of change of velocity are slightly larger for these instruments. The vector anemometers are mounted in an area of high air flow distortion and are intended for validation of the C.F.D. package and are not used for wind stress calculations. The rates of change of velocity are high, typically above 1.0 ms^{-1}/m, especially from the anemometers close to the areofoil. The Windmaster sonic and Young AQ anemometers mounted on the main mast have very low rates of change of velocity.

4.6 Conclusions

The foremast anemometers are mounted in a region of high rates of change of velocity and the percentage velocity errors range from -3.3 % for the sonic anemometers to -7.8 % for

the Young AQ foremast anemometers. The main mast Windmaster sonic and Young AQ anemometers over estimate the wind speed by 3.3 % and give very low rates of change of velocity in all three directions which suggests the results are reliable and the anemometers are in a well exposed position.

The Vector anemometers mounted above the bridge are in a region of high airflow disturbance. Across the four lowest vector anemometers the rate of change of velocity typically reads above 1.0 ms^{-1}/s. The areofoil above the bridge casts a large decelerated region approximately 5 m (Vector 2 and 5) above the monkey island and returns to an accelerated region at 6 m (Vector 1) above the deck, refer to Figure 7.

5. Charles Darwin cruise CD43.

5.1 Introduction

This section presents the errors in the wind speed measurements for the anemometer locations as employed during CD43. The model run used is 3.1/14, as in the previous sections, and the results are described in Sections 5.3 to 5.6. Section 5.7 compares these results with those from the earlier Darwin model, Moat and Yelland, (1995), run 1.6/13.

5.2 Anemometer locations

The anemometer locations (Figure 19) on Charles Darwin Cruise 43 were, in the model co-ordinate system:

Solent Sonic anemometer	(30.23, 15.15, -2.4)
Young propeller vane anemometer	(30.90, 15.65, -1.0)
Kaijo-Denki sonic anemometer	(32.1, 14.35, 1.6)
Bi-vane anemometer	(30.918, 15.7, 1.6)

5.3 Vertical displacement of the airflow

For the Solent sonic anemometer mounted on the port side of the foremast, the local plane is:

K19 z=-2.5806 m Solent sonic at z=-2.4 m

For the Solent sonic anemometer the airflow has been raised by 1.175 m from it's original height before it reaches the anemometer location (Table 12).

location	x (m)	y (m)	z (m)
Solent Sonic	30.23	15.15	-2.4
Z_{anemom}	30.15	15.155	-2.5806
Solent-Z_{anemom}	0.08	-0.005	0.1806
Z_{origin}	165.0	13.980	-2.5806
Z_{anemom}-Z_{origin}	-134.85	**1.175**	0

Table 12 Table showing the amount the air is raised when it reaches the Solent anemometer site.

For the Young propeller vane mounted on the port side of the foremast, the local plane is:

K21 z= -0.86597 m Young propeller vane at z=-1.0 m

For the Young propeller vane anemometer the airflow has been raised by 1.232 m from it's original height before it reaches the anemometer location (Table 13).

location	x (m)	y (m)	z (m)
Young	30.918	15.65	-1.0
Z_{anemom}	30.933	15.732	-0.86621
Young-Z_{anemom}	-0.015	-0.082	-0.134
Z_{origin}	190.33	14.5	-0.86597
Z_{anemom}-Z_{origin}	-159.346	**1.232**	0

Table 13 Table showing the amount the air is raised when it reaches the Young AQ anemometer site.

For the Kaijo Denki sonic mounted on the starboard side of the foremast, the local plane is:

K24 z = 1.7063 m Kaijo Denki sonic at z=1.6 m

For the Kaijo Denki sonic anemometer the airflow has been raised by 1.023 m from it's original height before it reaches the anemometer location (Table 14).

location	x (m)	y (m)	z (m)
Kaijo Denki sonic	32.10	14.35	1.6
Z_{anemom}	32.127	14.388	1.7063
Sonic-Z_{anemom}	-0.027	-0.038	-0.1063
Z_{origin}	191.05	13.365	1.7063
Z_{anemom}-Z_{origin}	-158.923	**1.023**	0

Table 14 Table showing the amount the air is raised when it reaches the Kaijo Denki sonic anemometer site.

For the Bi-vane mounted on the starboard side of the foremast, the local plane is:

K24 z = 1.7063m Bi-vane anemometer at z=1.6 m

For the Bivane anemometer the airflow has been raised by 1.174 m from it's original height before it reaches the anemometer location (Table 15).

location	x (m)	y (m)	z (m)
Bi vane anemometer	30.918	15.7	1.6
Z_{anemom}	30.943	15.734	1.7063
Bi vane-Z_{anemom}	-0.025	-0.034	-0.1063
Z_{origin}	190.12	14.560	1.7063
Z_{anemom}-Z_{origin}	-159.177	**1.174**	0

Table 15 Table showing the amount the air is raised when it reaches the Bivane anemometer site.

5.4 Free stream velocities

Free stream velocities, taken from the free stream plane, directly abeam of the anemometer locations are shown in Table 16.

Anemometer	Free stream velocity (m/s)	Height free stream velocity originated from (m)
Solent sonic	**14.074**	13.975
Young propeller vane	**14.103**	14.418
Kaijo Denki	**14.027**	13.327
Bi-vane	**14.111**	14.526

Table 16 Table showing the free stream velocities for each anemometer.

5.5 Velocities at anemometer locations

Figures 20 to 23 show the lines of data through the Solent sonic (port foremast), Young AQ (port foremast), Kaijo Denki (Stb. foremast) and Bivane (Stb. foremast) respectively. The percentage velocity errors for these sites are summarised in Table 17, and the rates of change of the velocity errors are shown in Table 18.

Anemometer	Velocity from each direction (m/s)	Average velocity (m/s)	Free stream velocity (m/s)	Wind speed error (%)	Vertical displacement (m)
Solent sonic	13.591 (x)				
	13.593 (y)	13.591	14.074	**-3.434**	1.175
	13.588 (z)				
Young	13.022 (x)				
	12.968 (y)	13.012	14.103	**-7.734**	1.232
	13.047 (z)				
Kaijo Denki	12.387 (x)				
	12.310 (y)	12.357	12.357	**-11.906**	1.023
	12.374 (z)				
Bi-vane	13.313 (x)				
	13.278 (y)	13.299	14.111	**-5.754**	1.174
	13.306 (z)				

Table 17 Velocity estimates at the anemometer sites

Anemometer	Velocity data line	Rate of change of velocity per meter (ms^{-1}/m)	Rate of change of velocity per cell (ms^{-1}/cell)
Solent sonic	along (x)	0.203	0.0290
	up (y)	0.110	0.00475
	across (z)	0.004	0.00935
Young	along (x)	0.520	0.0826
	up (y)	0.435	0.117
	across (z)	1.605	0.181
Kaijo Denki	along (x)	0.0300	0.0508
	up (y)	0.590	0.223
	across (z)	0.0615	0.131
Bivane	along (x)	0.310	0.0512
	up (y)	0.325	0.0909
	across (z)	0.030	0.0608

Table 18 Rates of change of velocity close to the anemometer sites

5.6 Comparison of results from Darwin model runs 3.1/14, 1.6/13 and 3.1/20

The Charles Darwin model was run using the same profile over two slightly different ship geometry's; 1) Vectis 1.6/13 modelled the flow over the Femgen DARWIN.G20 model which approximated the bridge aerofoil and Immarsat dome as solid blocks (Figure 1a), and 2) after ship visits, Femgen model DAR96.G20 (Figure 1b) was produced with more realistic geometry and used for the Vectis run 3.1/14. The velocity errors and vertical displacements of the airflow from each run using the re-analysis of 1.6/13 (Moat and Yelland, 1995) are summarised in Table 19.

The vertical displacement of the air flow is approximately 0.20 m greater for the Solent sonic and Young AQ anemometers and approximately 0.14 m for the Kaijo Denki sonic and the Bivane anemometers using the modified geometry of Vectis run 3.1/14. The percentage error is reduced for the Solent sonic anemometer (1.081 %), whilst the percentage error is virtually unchanged for the Young AQ (0.083 %) and increased for the Kaijo Denki sonic (1.619 %). These differences between the two runs could be attributed to;.

1) the changes in the ship geometry

2) the different resolutions in mesh density (Figures 24 and 25)

3) the differences between versions 1.6 and 3.1 of phase 5 of Vectis

4) the change in the vertical wind profile upstream of the ship (the profiles were identical abeam of the foremast).

To investigate this problem further, a third simulation of the Darwin was performed (Vectis run 3.1/20). Run 3.1/20 used exactly the same mesh density and geometry as run 1.6/13, but was run using version 3.1 of phase 5 and used the same profile as run 3.1/14. The results from run 3.1/20 are also summarised in Table 19.

Anemom-eter	1.6/13 re-analysis		3.1/14		3.1/20	
	% Error	Height the air raised (m)	% Error	Height the air raised (m)	% Error	Height the air raised (m)
Solent sonic	-4.515	0.947	-3.434	1.175	-4.251	1.168
Young propeller vane	-7.651	1.024	-7.734	1.232	-8.137	1.183
Kaijo Denki	-10.287	0.885	-11.906	1.023	-10.242	1.013
Bivane	-	-	-5.754	1.174	-6.106	1.143

Table 19 Summary of velocity errors from Vectis runs 1.6/13, 3.1/14 and 3.1/20 over the Charles Darwin.

The wind speed errors are similar for the two runs with the same geometry and mesh density (1.6/13 and 3.1/20), and differ for run 3.1.14 where the geometry and mesh were changed. The results for the Young seem slightly anomalous, but this anemometer was situated in a region where the velocity was changing rather rapidly. It would be reasonable to assume that changes in the geometry of the bridge would affect all the anemometer sites in the same sense, if not to the same degree, i.e. the improvement in the aerofoil may have reduced the blockage to the flow and hence lessened the deceleration of the flow at the foremast. However, the sign of the change in the wind speed error depends on the anemometer site: it seems likely that the change in the mesh density is the cause of the differences in wind speed error, rather than the change in the geometry. For example, Figure 21 shows the velocity in the region of the Young propeller vane anemometer. It can be seen that the velocity depends non-linearly with distance from the anemometer site, and that the use of a coarser mesh may give different results. This confirms the earlier result that the wind speed error has only a weak dependence on the shape of the profile: for the CSS Hudson, the error at the bow anemometer increased from -2.9% to -3.7% (at the main mast from +8.1% to +6.0%) when the profile was changed from uniform to logarithmic (Hutchings *et al.*, 1995).

In contrast, the values for the vertical displacements seem to depend on the version of phase 5 and the vertical profile, rather than on the mesh or geometry details. It is not surprising that the changes in mesh density and ship geometry have no apparent effect, since these changes were very localised and the vertical displacement is determined by the flow upstream of the ship. Staff at Ricardo Engineering Consultants Ltd. (the producers of Vectis) state that there is no difference between versions 1.6 and 3.1 of phase 5, as far as the parameterisation of the flow is concerned. However, in version 1.6 of phase 5, a logarithmic input profile degraded significantly along the length of the tunnel, becoming more uniform with distance (Hutchings, 1995). This was attributed by Ricardo to a problem with the indirect addressing. Each cell has a roughness element assigned to it in an array and the addressing did not always point to the right place in the array. This affected the calculation of the shear stress, and hence the shape of the profile. In this way, the shape of the profile and the turbulence calculations both depend on the version of phase5 used.

The accuracy of the wind speed errors from the Vectis code are increased if extracted from Version 3.1, using a tight mesh in regions of high rates of change of velocity. Hence, the results from run 3.1/14 are regarded as the most accurate, and are discussed in section 6.

6. Summary

The comparisons of the different simulations of the flow over the Darwin show that it is necessary to have sufficient mesh density in areas where the velocity field varies rapidly. If the mesh is too coarse, the calculated wind speed errors will not be accurate. The comparisons also suggest that the vertical displacement of the flow could be dependent on the shape of the wind profile. The results from Charles Darwin 3.1/14 are summarised in this section.

For Charles Darwin cruises CD98 (passage leg) and CD98a the measured wind speed is reduced from the free stream value by 3.4 % and 3.3 % for the fast sampling Research sonic and Wind master sonic respectively. The Young AQ anemometers exhibit slightly larger reductions from the free stream, Port Young AQ 7.8 % and Starboard Young AQ 5.1 %. The rates of change of velocity in the foremast region are quite high; the maximum rate of -0.188 ms^{-1}/cell for the port Young anemometer would give an error in the wind speed estimate of -7.7$\pm$ 1.3 % in $\pm$1 cell (approximately $\pm$0.21m), across the anemometer site. The five Vector anemometers mounted above the ships bridge were placed in a region of high velocity error for future validation of the C.F.D. package Vectis. Wind speed data logged by the main mast Wind master sonic and Young AQ anemometers both overestimate the free stream value by 3.4 %. The rates of change of velocity are very low, less than 0.04 ms^{-1}/cell, which show that these anemometers were in a well exposed position.

The study of the wind speed errors on Charles Darwin cruises CD43 showed the anemometers mounted on the foremast to be in a region of severely decelerated flow, with a wind speed error of -3.4% for the Solent sonic and -11.9 % for the Kaijo-Denki. The rates of change of velocity were rather high; the maximum rate of -0.181 ms^{-1}/cell for the port young propeller vane anemometer would give an error in the wind speed of -7.5$\pm$1.3 % in $\pm$1 cell (approximately $\pm$0.21m), across the anemometer site.

7. References

Hutchings, J. 1995. *Airflow over the R.R.S. Charles Darwin*, Vectis report 1.6/13, Southampton Oceanography Centre, (Unpublished Report).

Hutchings, J., Yelland, M. J. and Taylor, P. K. 1995. *A preliminary Computational Fluid Dynamics analysis of the airflow over the C.S.S. Hudson*, Canadian Contract Report, James Rennell Centre, Southampton, U. K.

Moat, B. I. and Yelland, M. J. 1995. *Airflow over the R.R.S. Charles Darwin (A re analysis of Vectis run 1.6/13)*, Vectis Report 1.6/13a, Southampton Oceanography Centre, (Unpublished Report).

Moat, B. I., Yelland, M. J. and Hutchings, J. 1996. *Airflow over the R.R.S. Discovery using the Computational Fluid Dynamics package Vectis*, SOC Internal report 2, Southampton Oceanography Centre, Southampton, U.K.

Yelland, M. J., Moat, B. I., Taylor, P. K., Pascal, R. W., Hutchings, J. and Cornell, V. C. 1996. 'Measurements of the open ocean drag coefficient corrected for airflow disturbance by the ship.', submitted to *Boundary Layer Meteorology*.

8. Figures

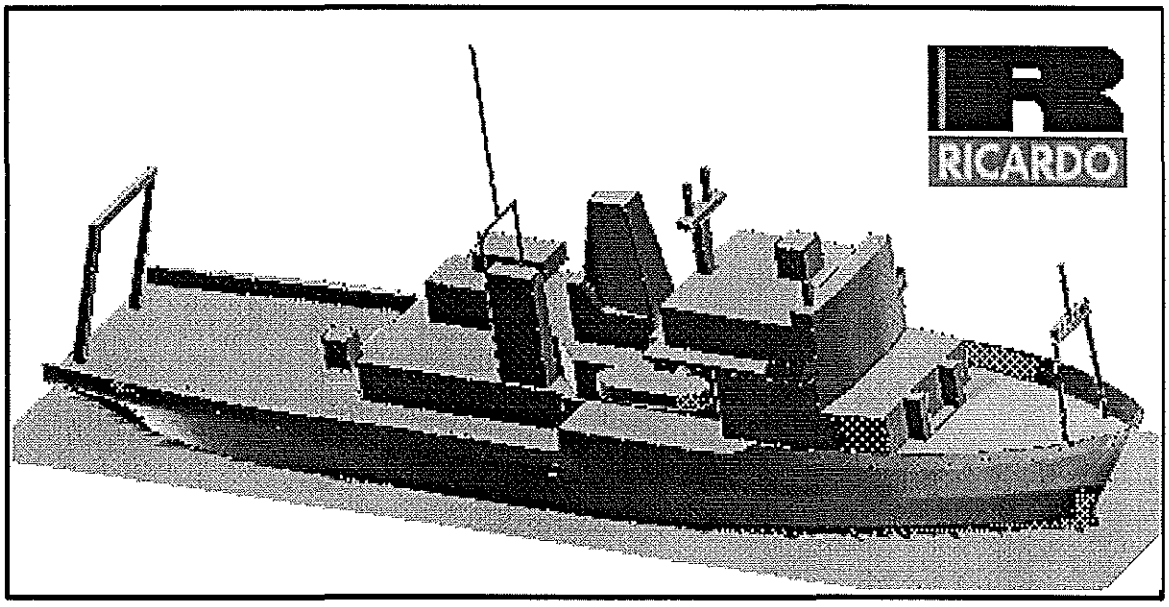

Figure 1 a) The R.R.S. Charles Darwin (Vectis run 1.6/13) Femgen model DARWIN.G20.

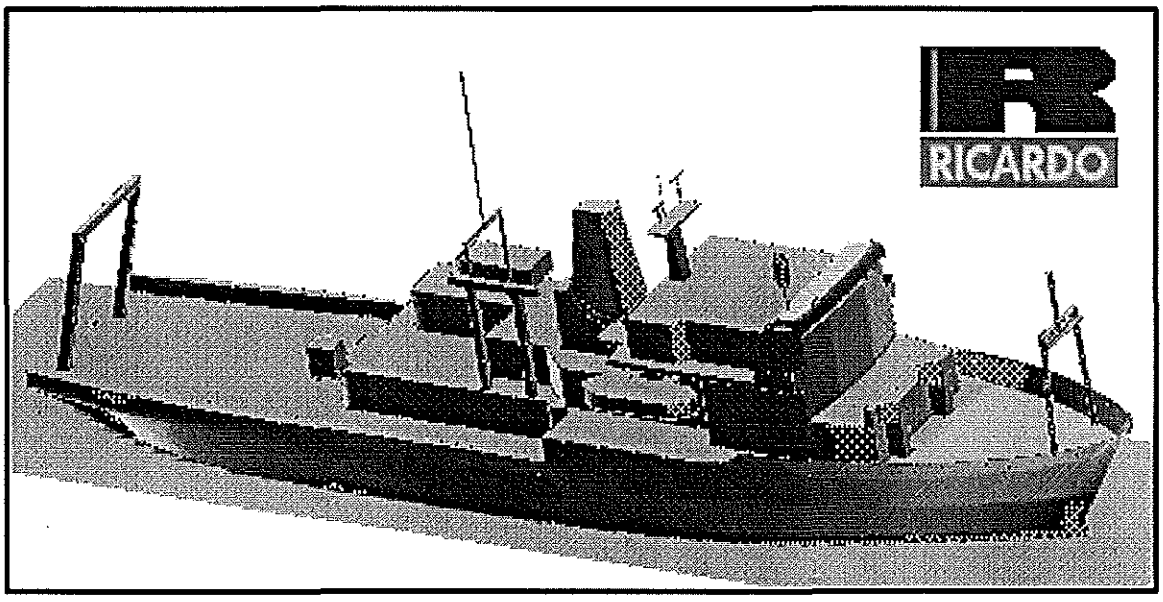

Figure 1 b) The R.R.S. Charles Darwin (Vectis run 3.1/14) Femgen model DAR96.G20.

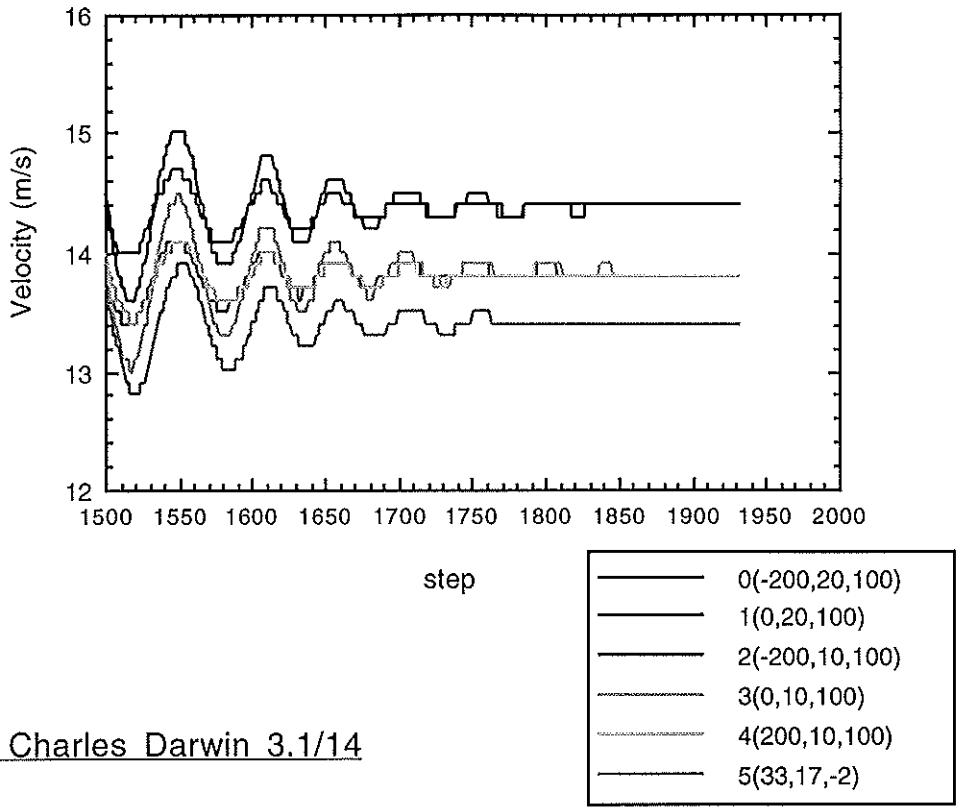

Figure 2 The total velocity for each monitoring location in Vectis run 3.1/14 (10m wind speed of 13.8 m/s).

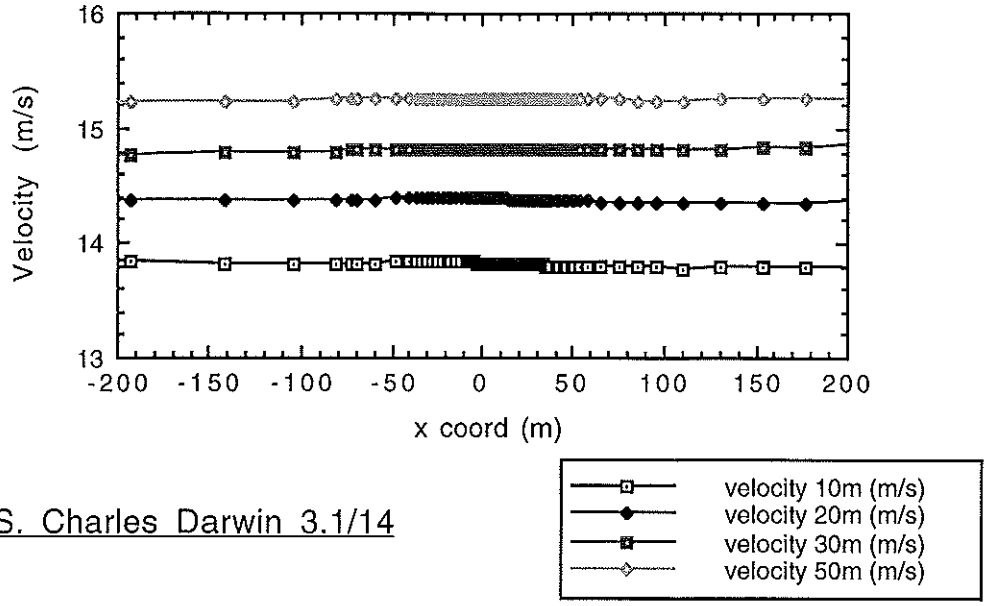

Figure 3a) Free stream velocities at heights of 10m, 20m, 30m and 50 m.

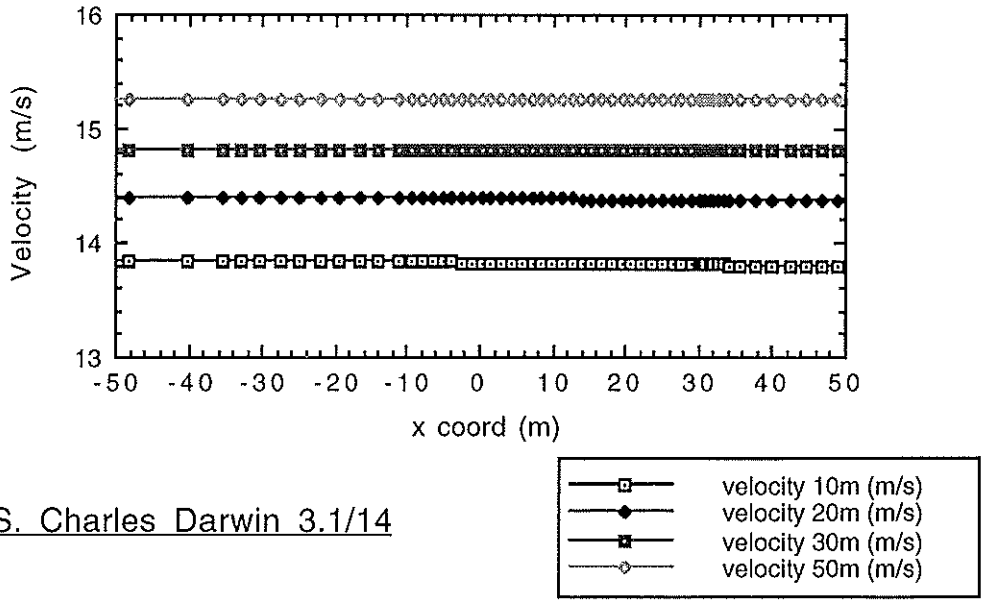

Figure 3b) Free stream velocities abeam of the ship.

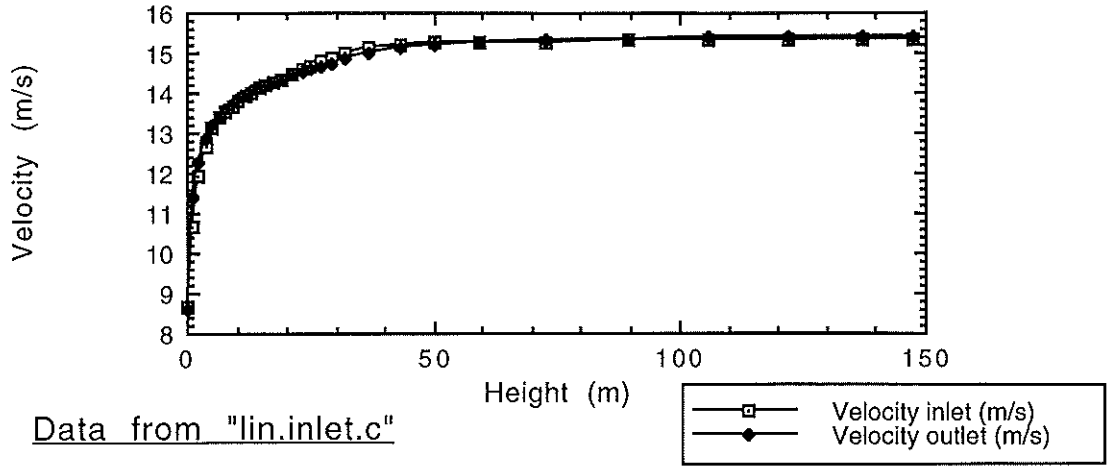

Figure 4 Wind profiles close to the inlet (250, 0<y<150, 100) and close to the outlet (-250, 0<y<150, 100).

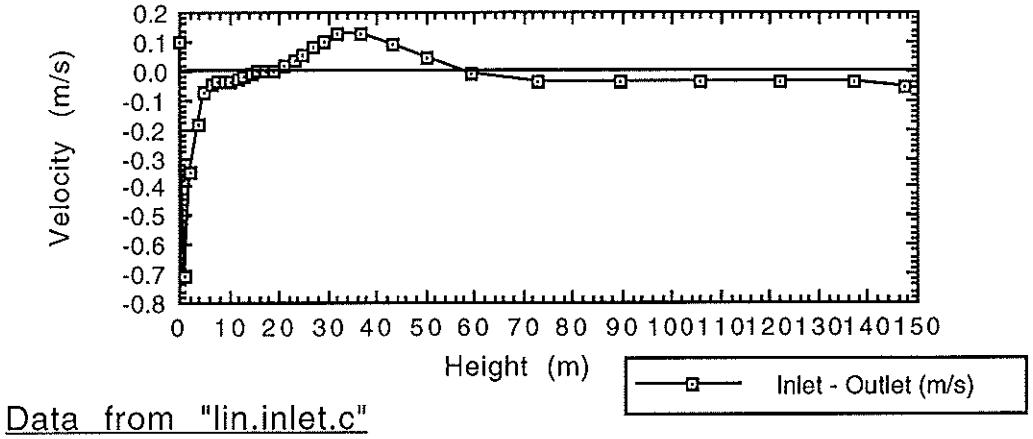

Figure 5 The difference between the velocity at the inlet and outlet.

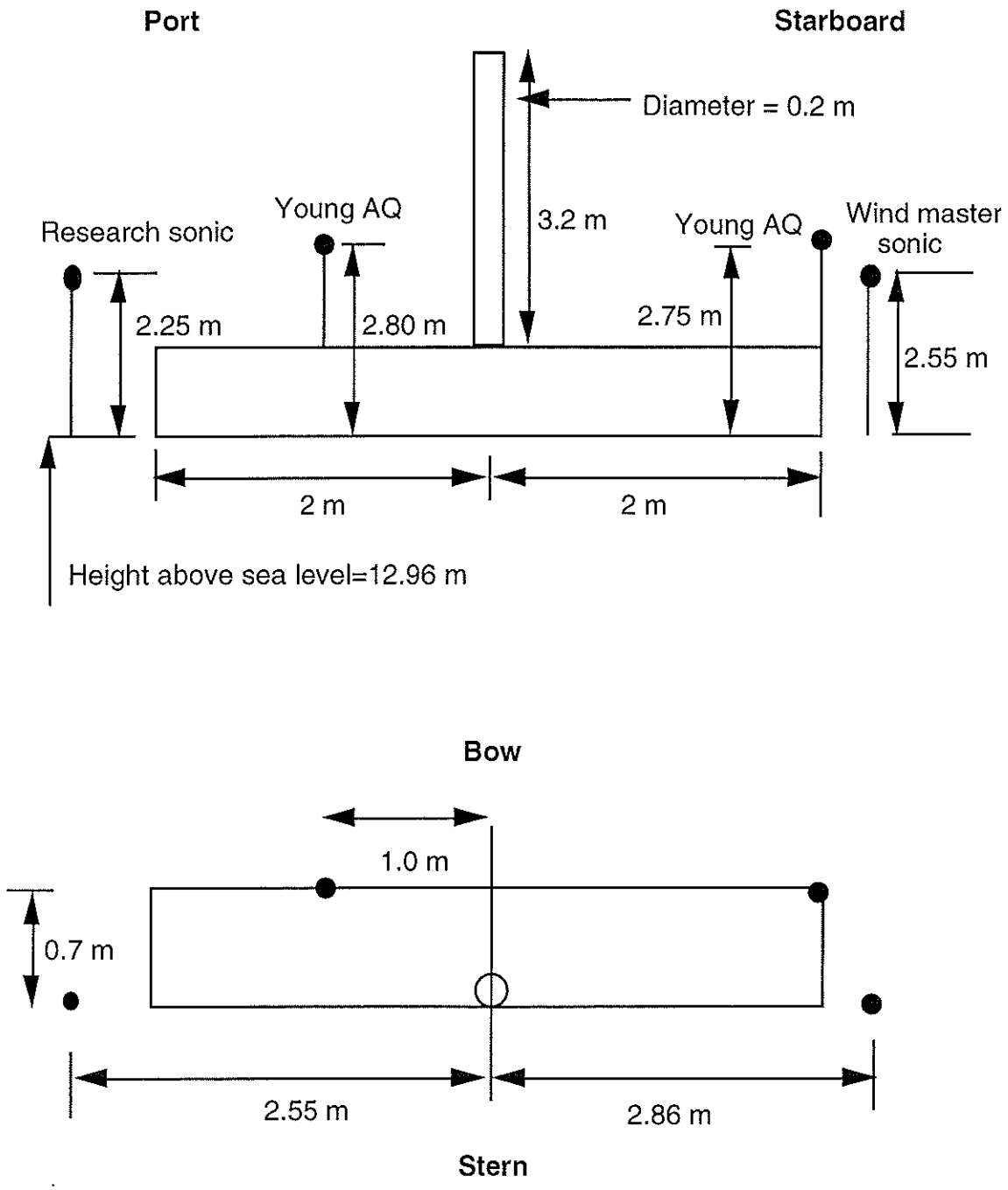

Note : Not to scale

Figure 6 The locations of the foremast anemometers on Charles Darwin CD98 and CD98a.

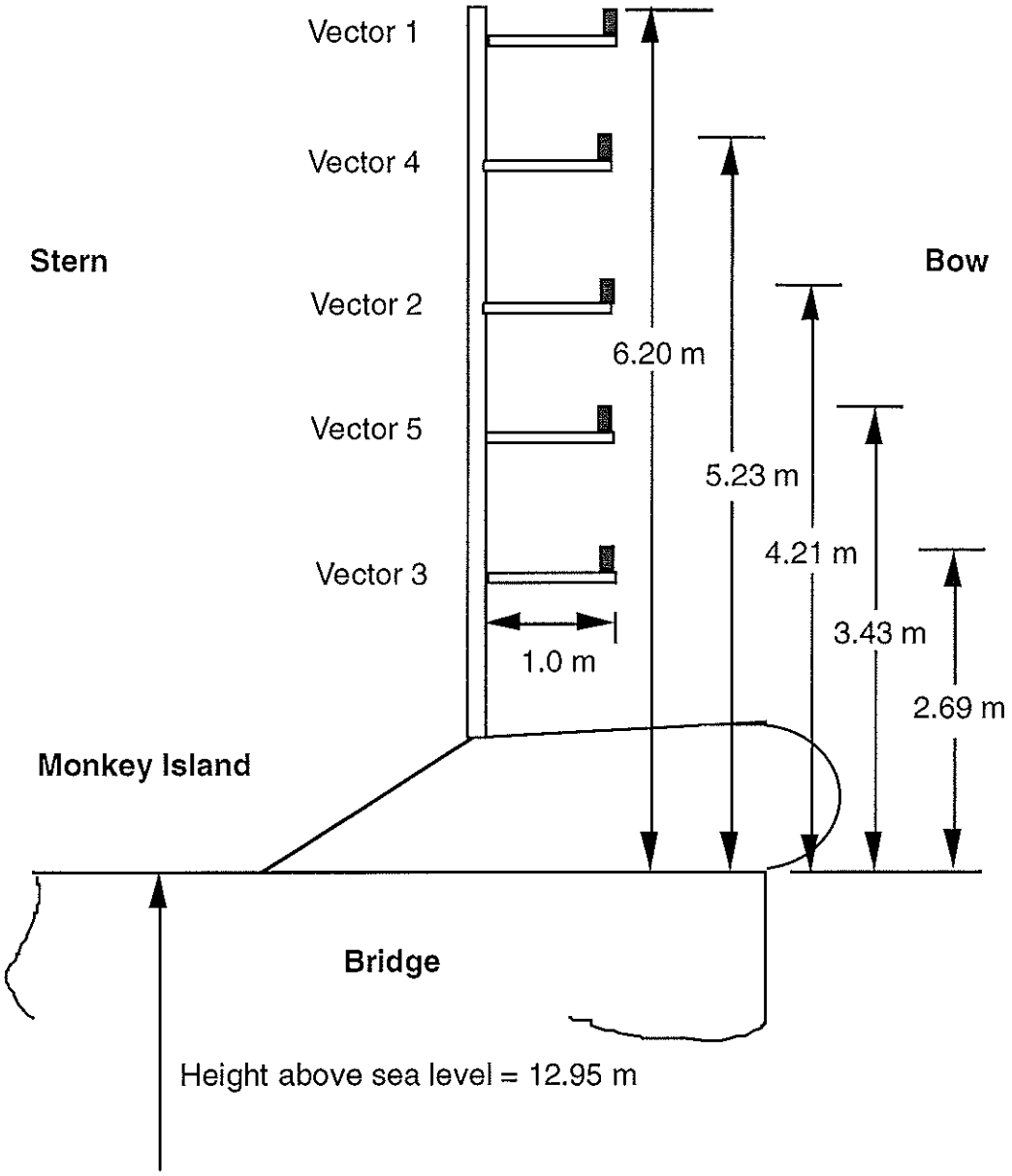

Note : Not to scale

Figure 7 The locations of the vector anemometers on CD98 and CD98a.

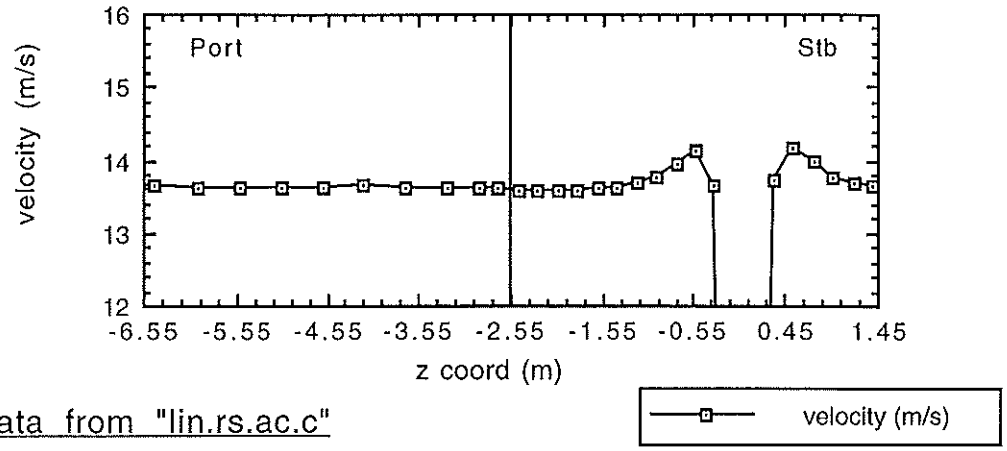

Figure 8 a) Velocity of 13.597 m/s across the port Research sonic anemometer on CD98 and CD98a.

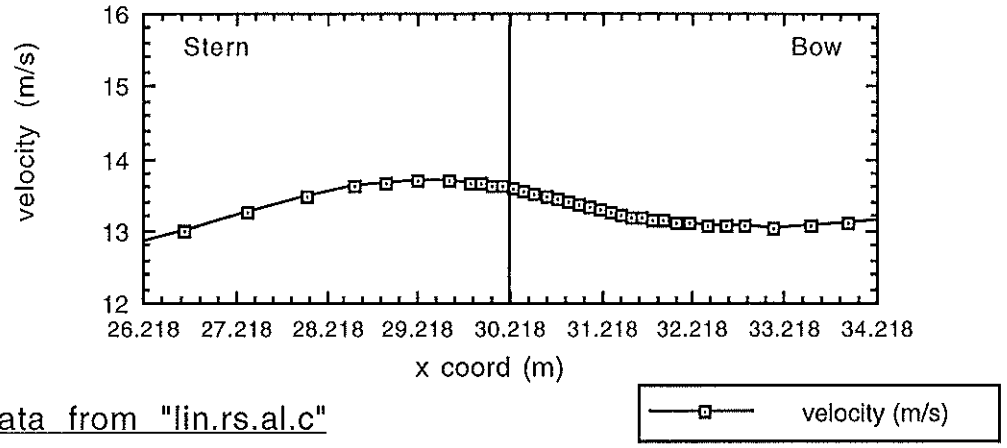

Figure 8 b) Velocity of 13.591 m/s along the port Research sonic anemometer on CD98 and CD98a.

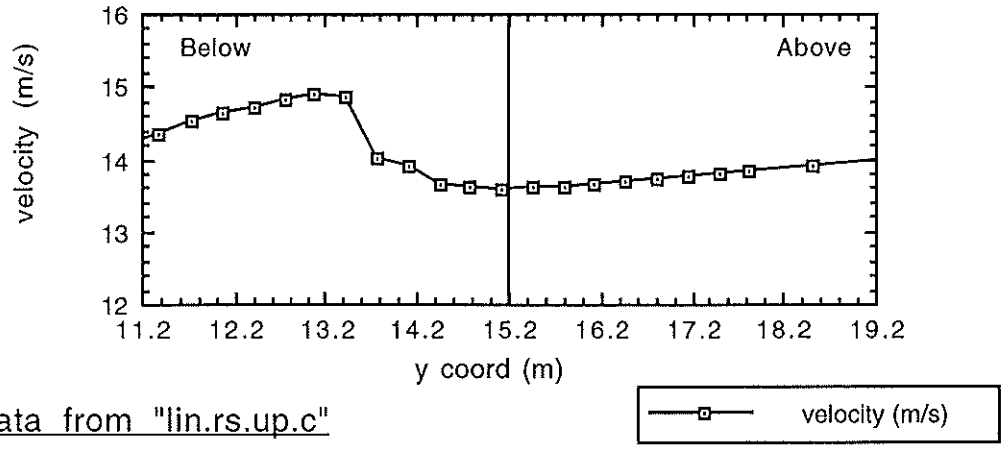

Figure 8 c) Velocity of 13.595 m/s through the port Research sonic anemometer on CD98 and CD98a.

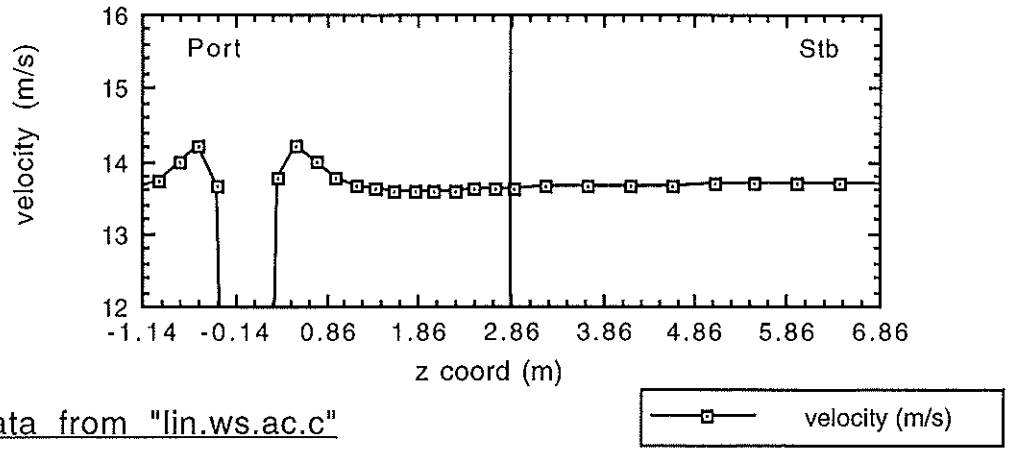

Figure 9 a) Velocity of 13.628 m/s across the Stb. Windmaster sonic anemometer on CD98 and CD98a.

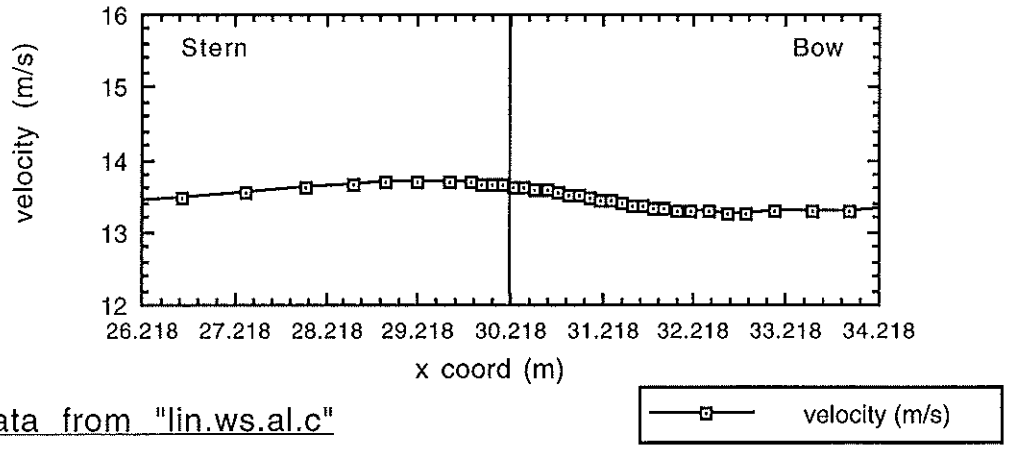

Figure 9 b) Velocity of 13.629 m/s along the Stb. Windmaster sonic anemometer on CD98 and CD98a.

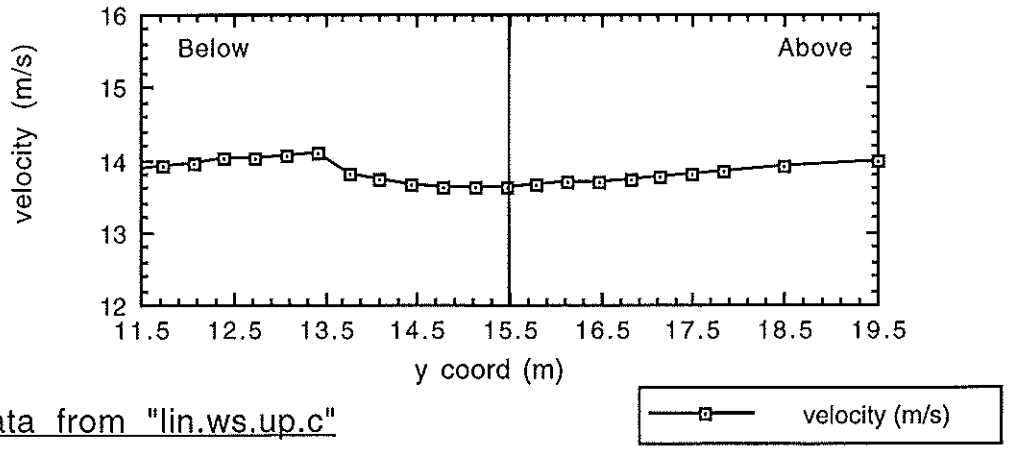

Figure 9 c) Velocity of 13.632 m/s through the Stb. Windmaster sonic anemometer on CD98 and CD98a.

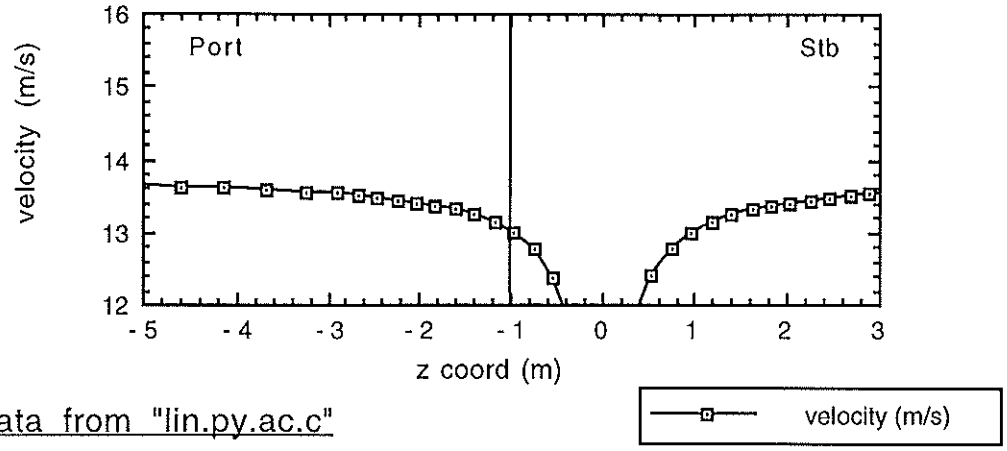

Figure 10 a) Velocity of 13.026 m/s across the port Young AQ anemometer on CD98 and CD98a.

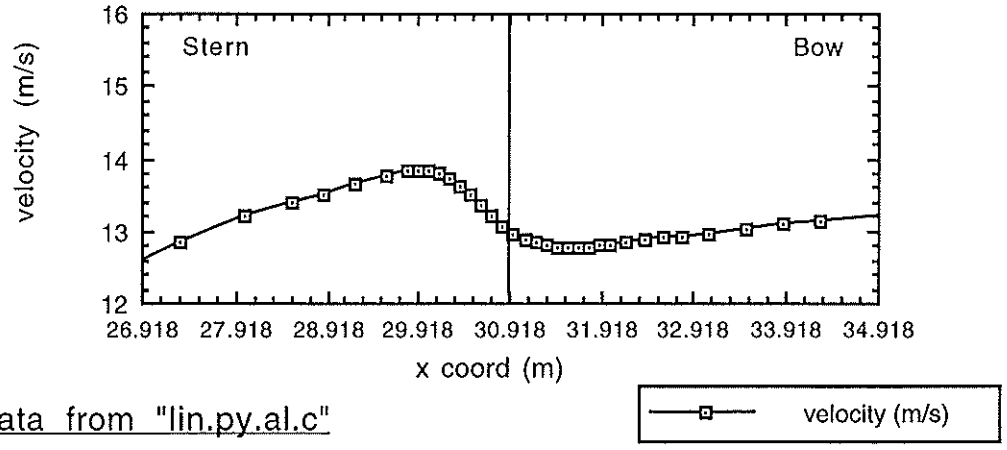

Figure 10 b) Velocity of 13.005 m/s along the port Young AQ anemometer on CD98 and CD98a.

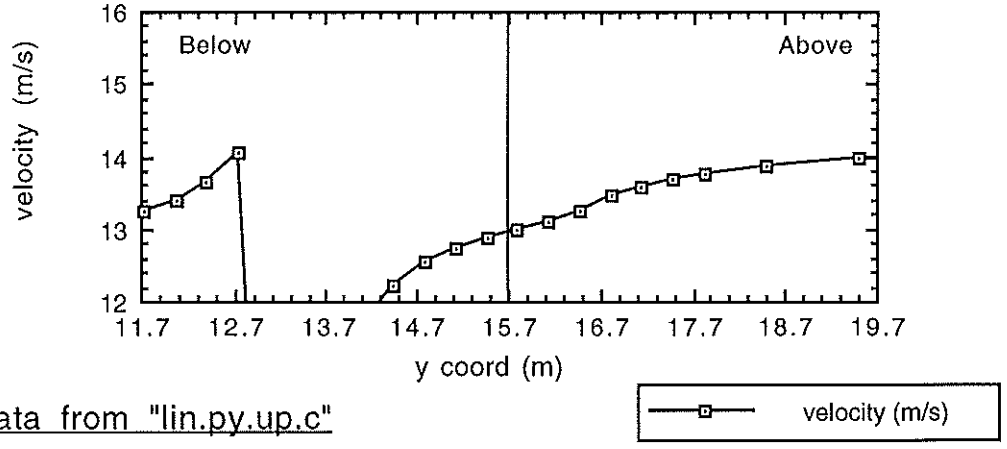

Figure 10 c) Velocity of 12.958 m/s through the port Young AQ anemometer on CD98 and CD98a.

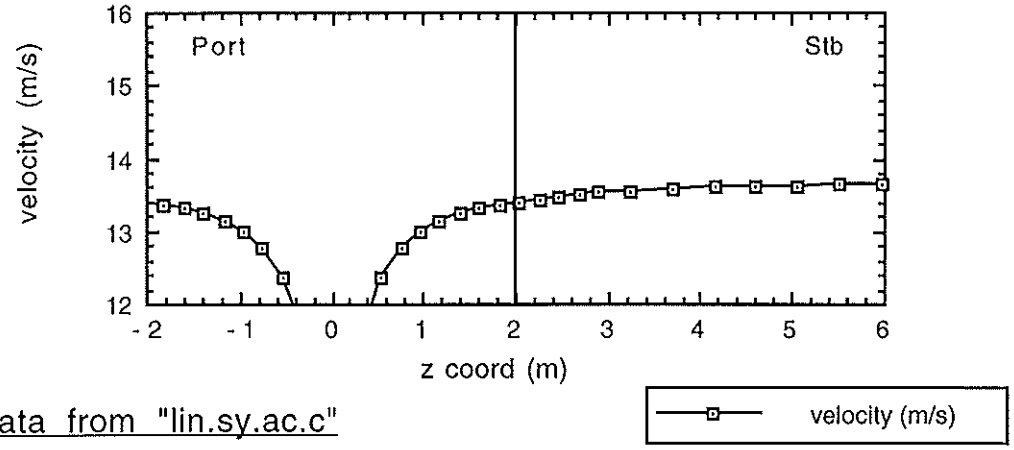

Figure 11 a) Velocity of 13.399 m/s across the stb. Young AQ anemometer on CD98 and CD98a.

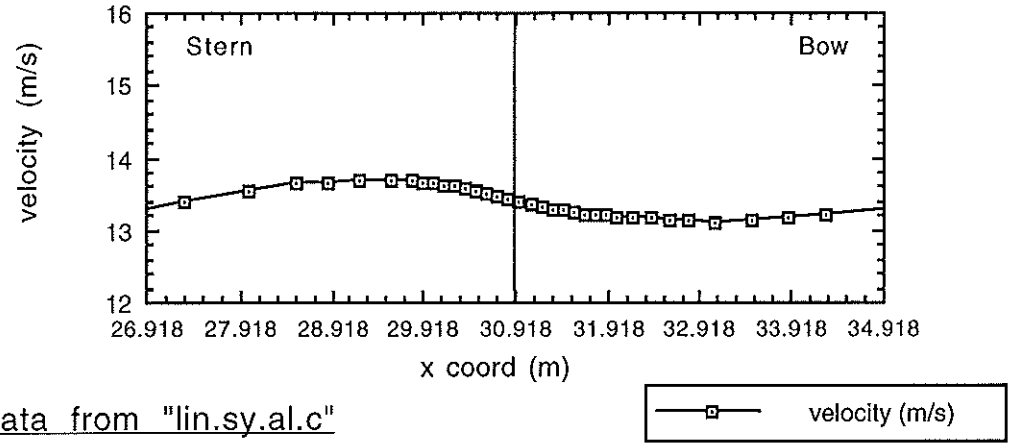

Figure 11 b) Velocity of 13.407 m/s along the stb. Young AQ anemometer on CD98 and CD98a.

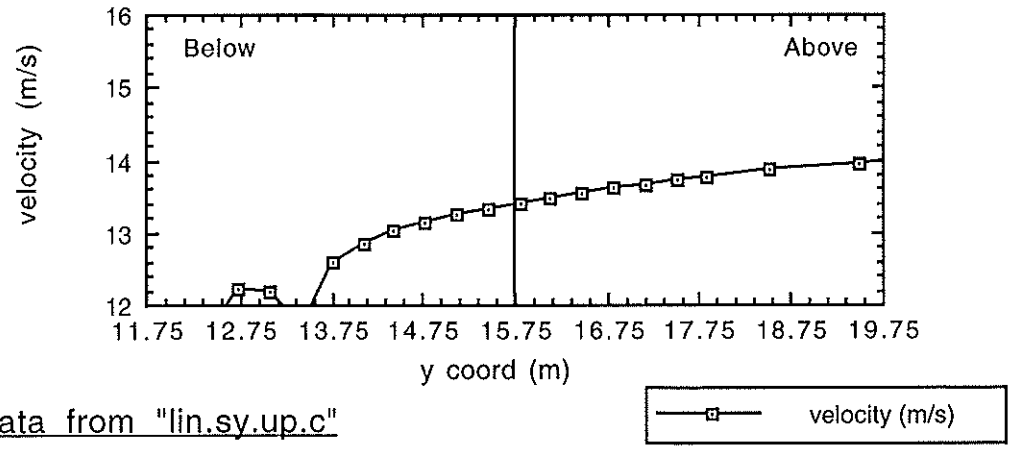

Figure 11 c) Velocity of 13.396 m/s through the stb. Young AQ anemometer on CD98 and CD98a.

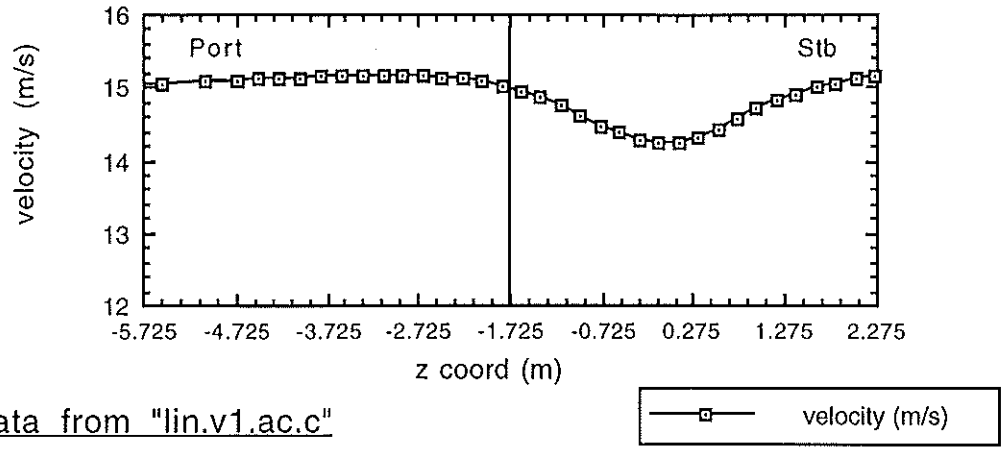

Figure 12 a) Velocity of 14.985 m/s across the first vector anemometer on CD98 and CD98a.

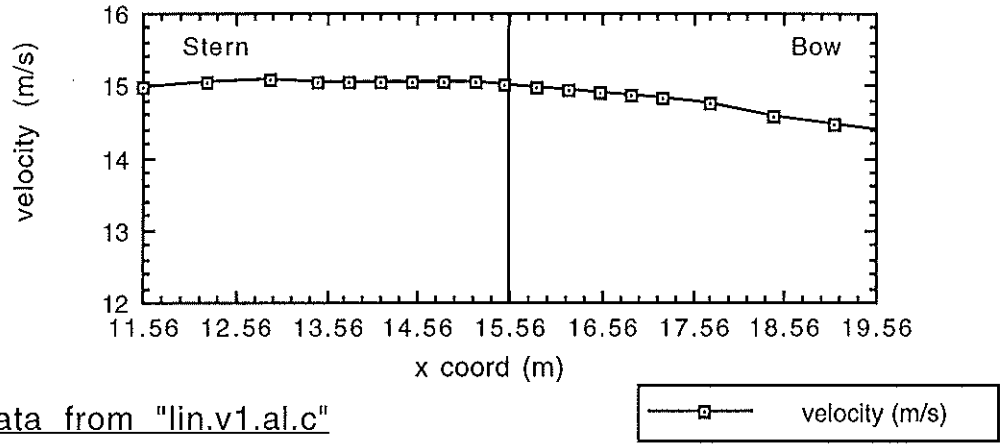

Figure 12 b) Velocity of 15.017 m/s along the first vector anemometer on CD98 and CD98a.

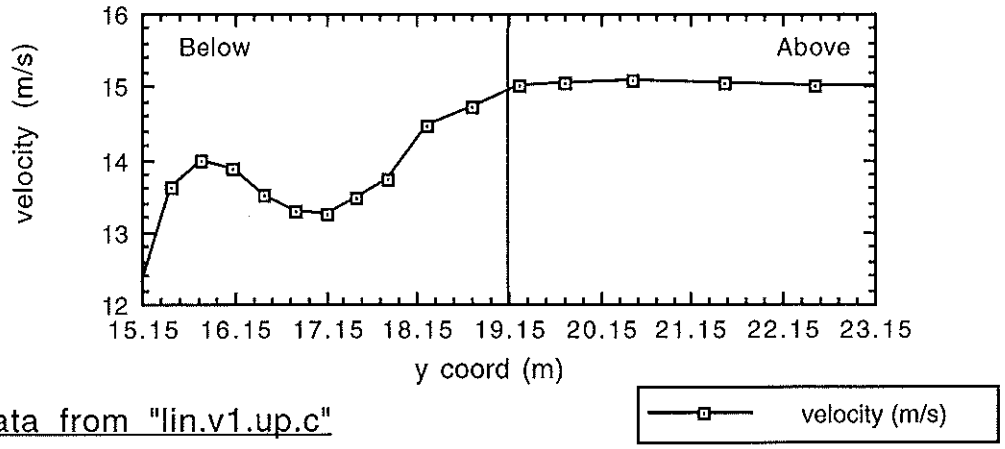

Figure 12 c) Velocity of 14.957 m/s through the first vector anemometer on CD98 and CD98a.

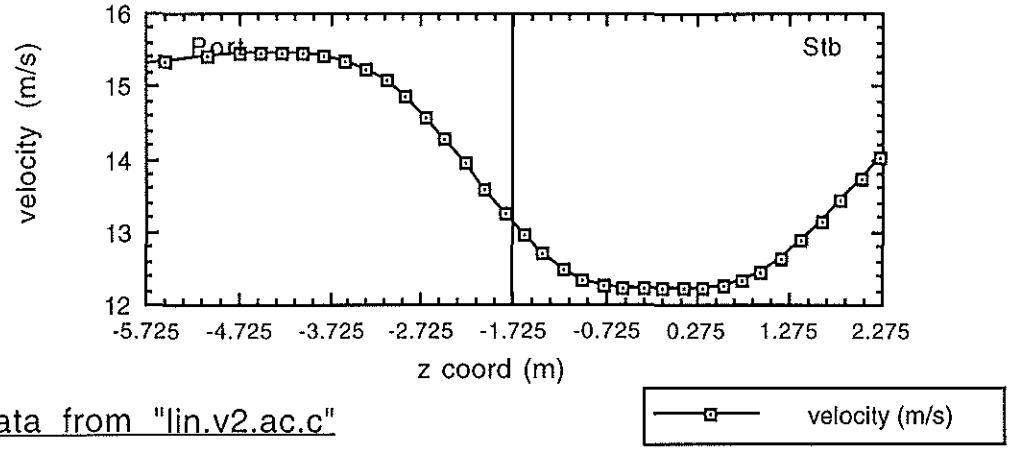

Figure 13 a) Velocity of 13.110 m/s across the second vector anemometer on CD98 and CD98a.

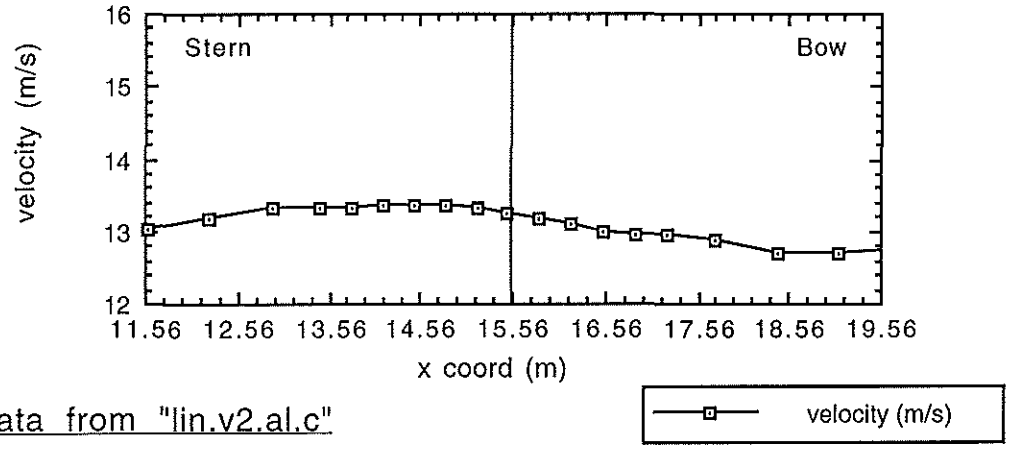

Figure 13 b) Velocity of 13.255 m/s along the across vector anemometer on CD98 and CD98a.

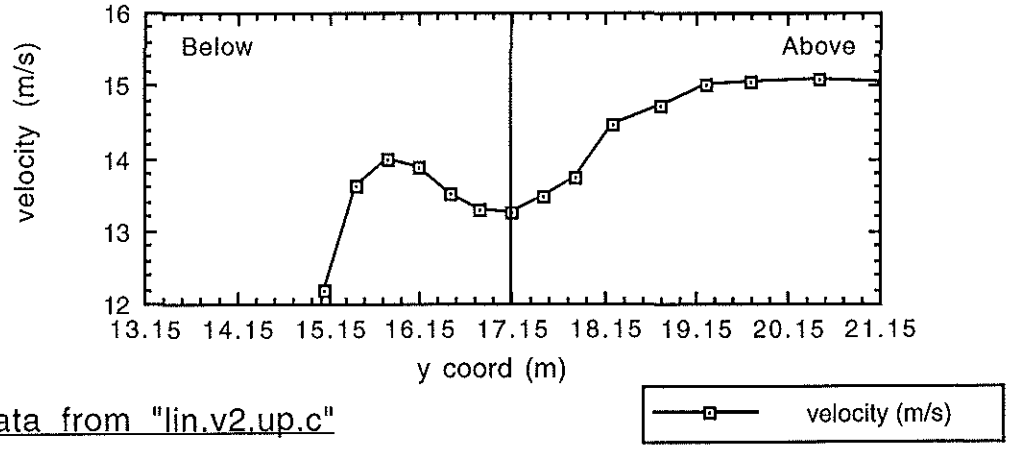

Figure 13 c) Velocity of 13.252 m/s through the second vector anemometer on CD98 and CD98a.

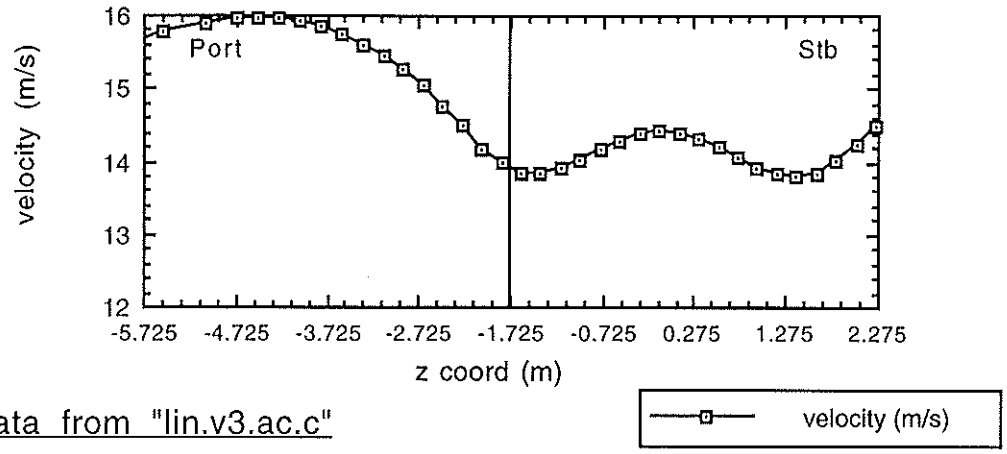

Figure 14 a) Velocity of 13.922 m/s across the third vector anemometer on CD98 and CD98a.

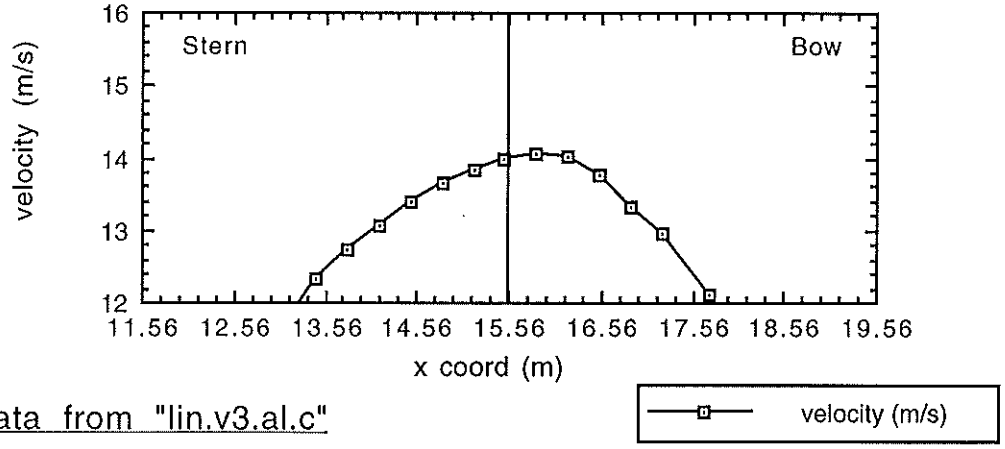

Figure 14 b) Velocity of 13.922 m/s along the third vector anemometer on CD98 and CD98a.

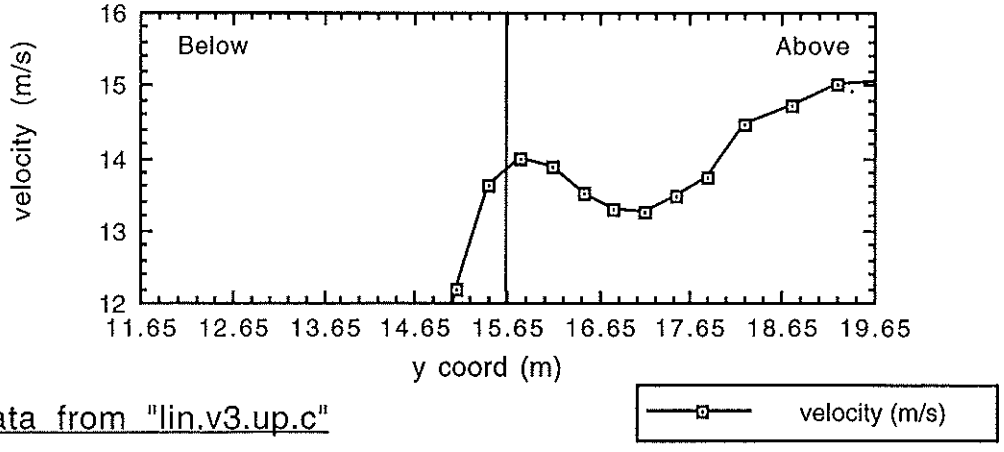

Figure 14 c) Velocity of 13.816 m/s through the third vector anemometer on CD98 and CD98a.

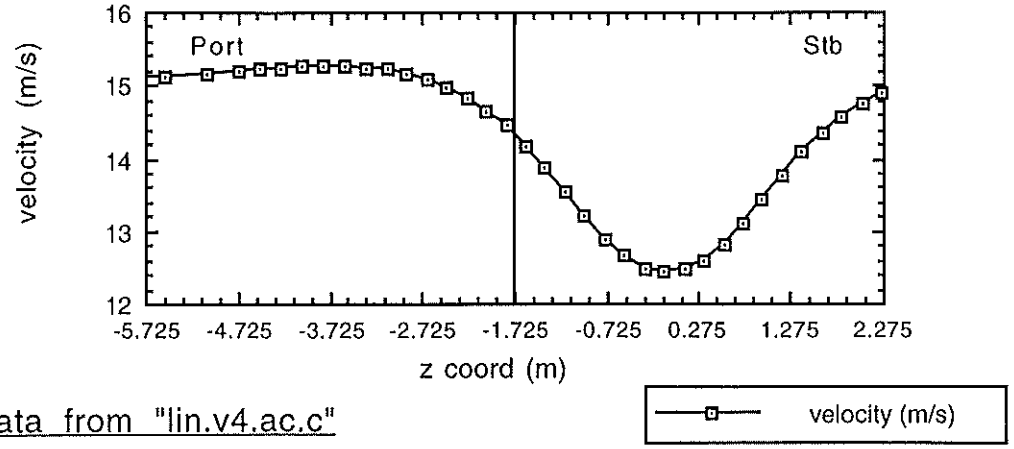

Figure 15 a) Velocity of 14.445 m/s across the fourth vector anemometer on CD98 and CD98a.

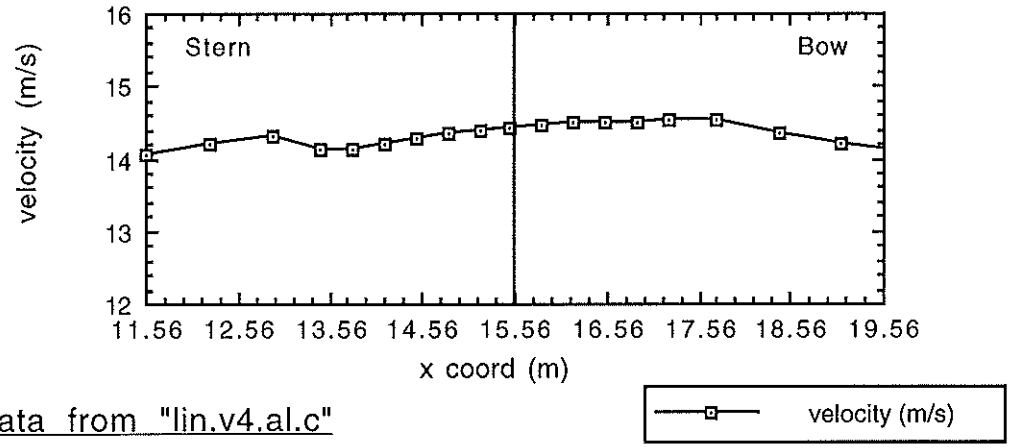

Figure 15 b) Velocity of 14.444 m/s along the fourth vector anemometer on CD98 and CD98a.

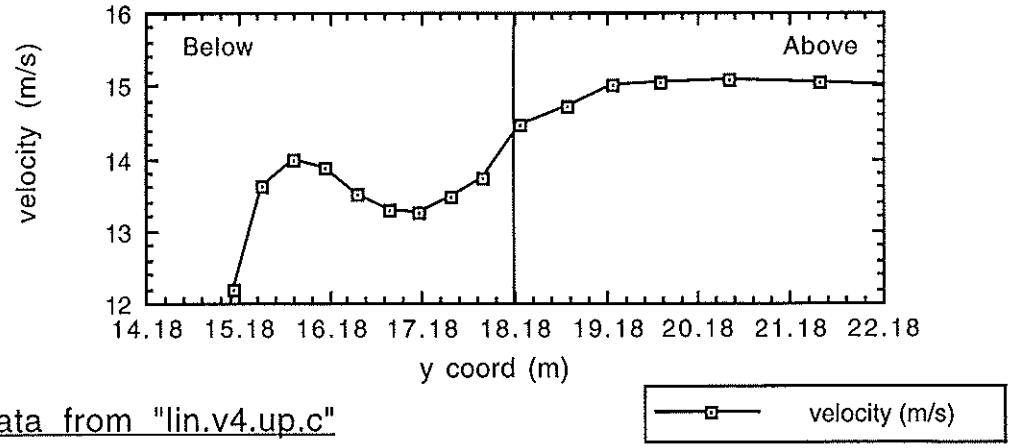

Figure 15 c) Velocity of 14.312 m/s through the fourth vector anemometer on CD98 and CD98a.

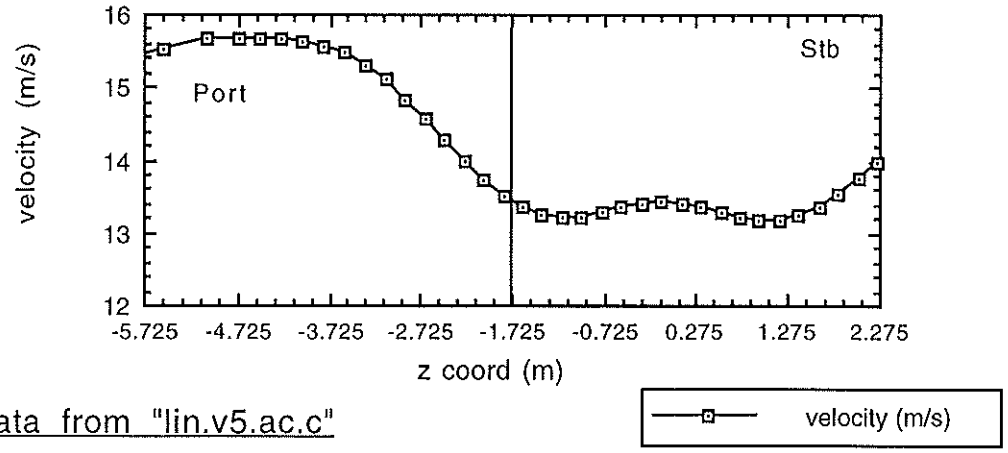

Figure 16 a) Velocity of 13.440 m/s across the fifth vector anemometer on CD98 and CD98a.

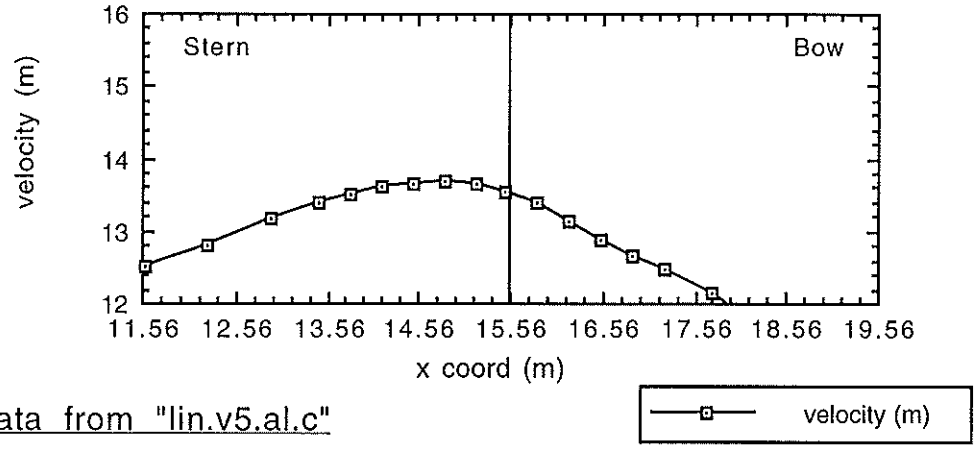

Figure 16 b) Velocity of 13.594 m/s along the fifth vector anemometer on CD98 and CD98a.

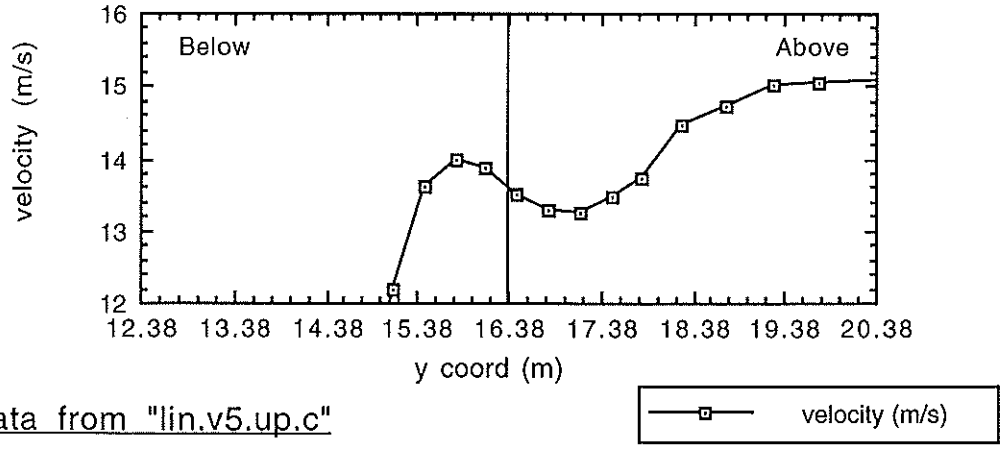

Figure 16 c) Velocity of 13.594 m/s through the fifth vector anemometer on CD98 and CD98a.

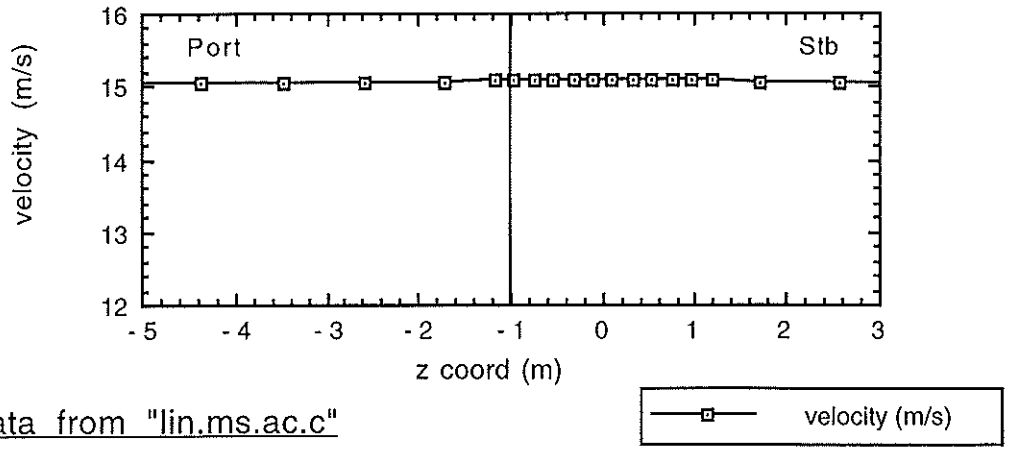

Figure 17 a) Velocity of 15.070 m/s across the main mast Windmaster sonic anemometer on CD98 and CD98a.

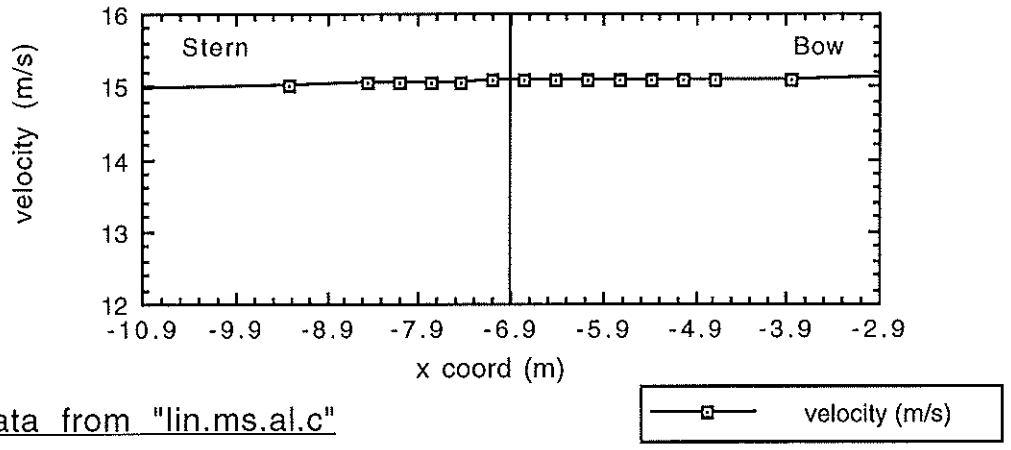

Figure 17 b) Velocity of 15.069 m/s along the main mast Windmaster sonic anemometer on CD98 and CD98a.

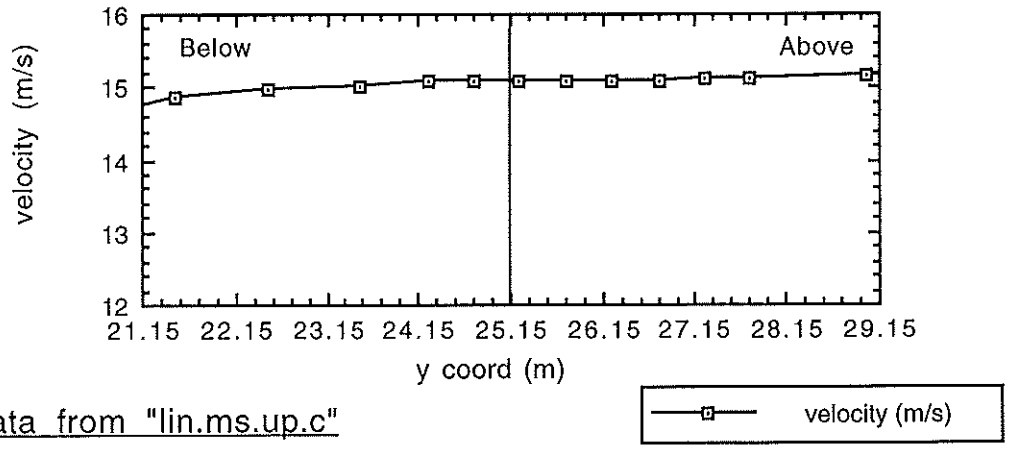

Figure 17 c) Velocity of 15.071 m/s through the main mast Windmaster sonic anemometer on CD98 and CD98a.

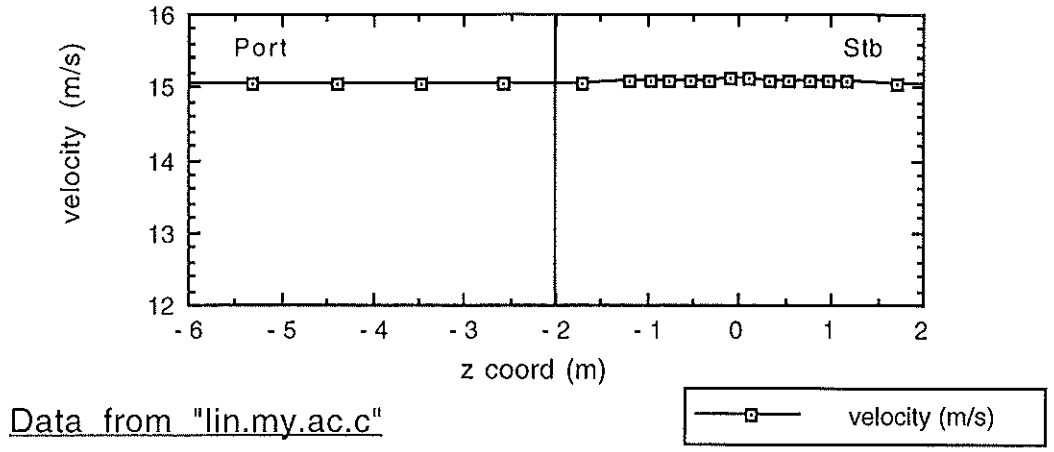

Figure 18 a) Velocity of 15.052 m/s across the main mast Young AQ anemometer on CD98 and CD98a.

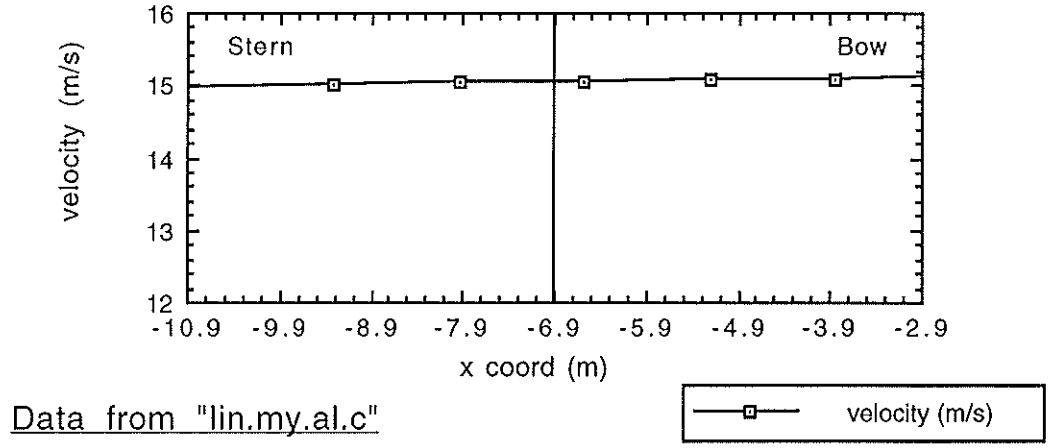

Figure 18 b) Velocity of 15.053 m/s along the main mast Young AQ anemometer on CD98 and CD98a.

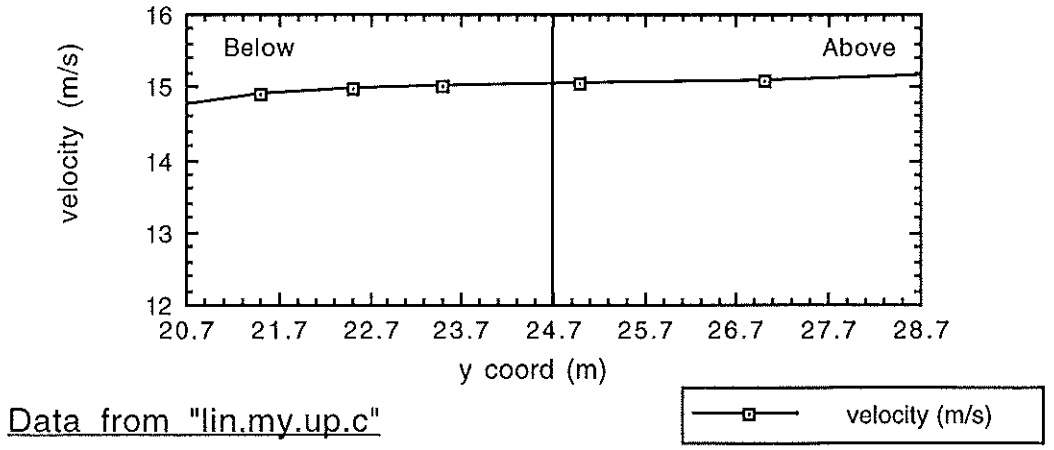

Figure 18 c) Velocity of 15.045 m/s through the main mast Young AQ anemometer on CD98 and CD98a.

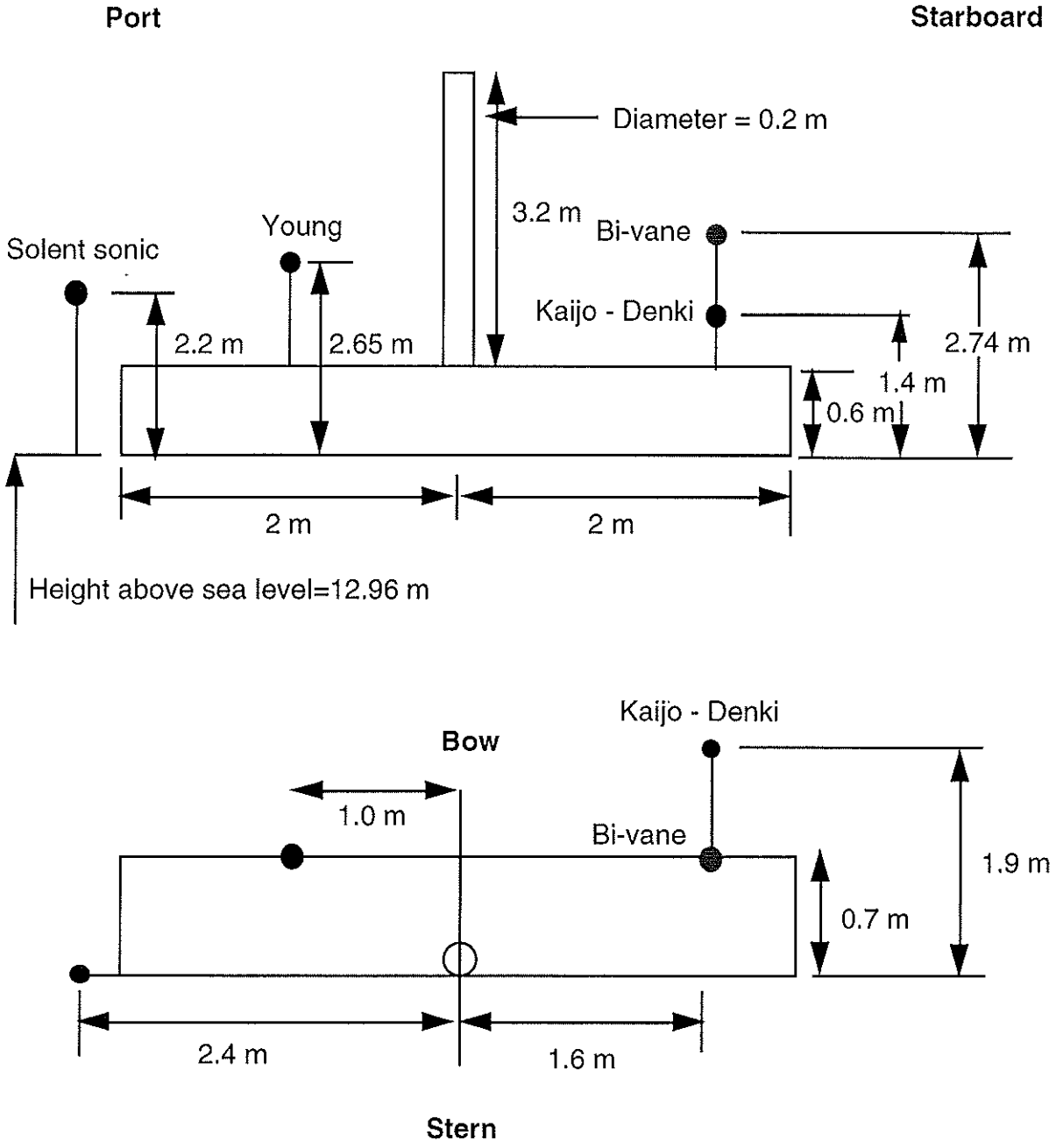

note : Not to scale

Figure 19 The locations of the anemometers relative to the foremast on R.R.S. Charles Darwin CD43.

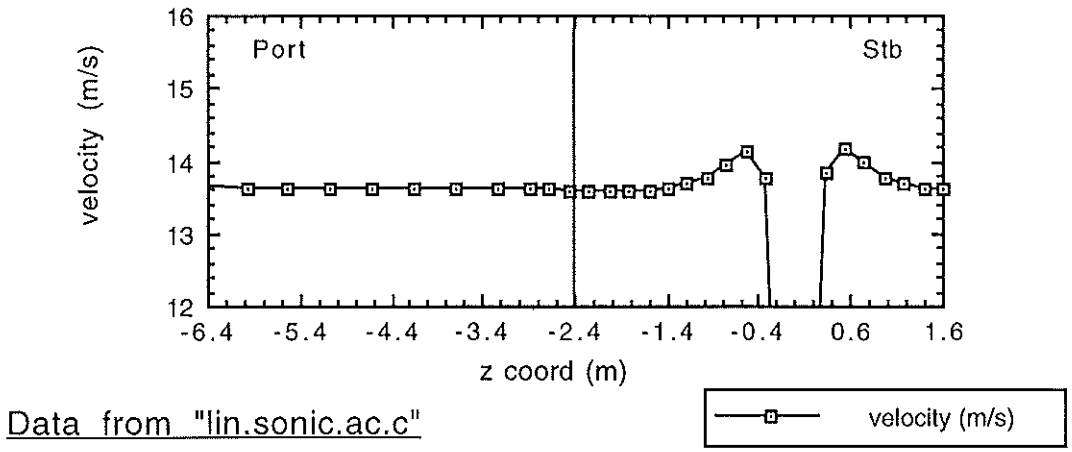

Figure 20 a) Velocity of 13.588 m/s across the Solent sonic anemometer on CD43.

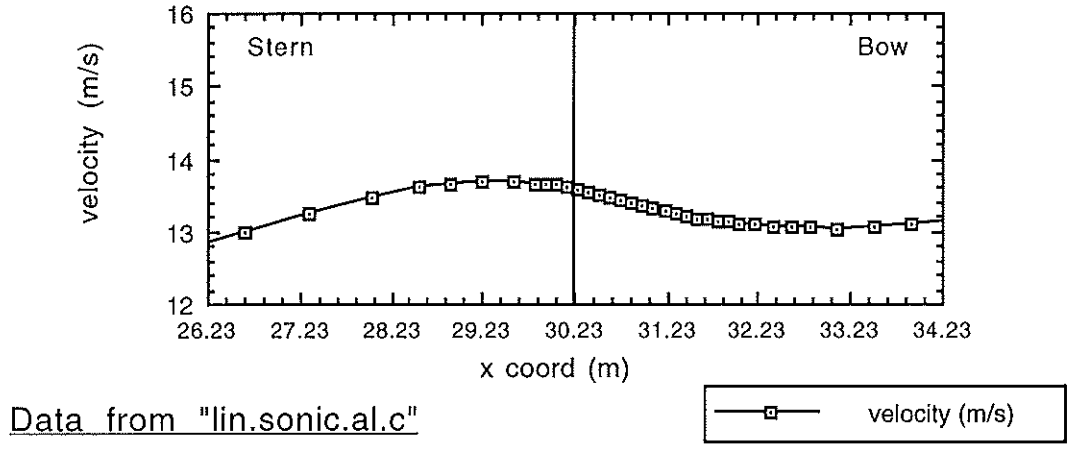

Figure 20 b) Velocity of 13.591 m/s along the Solent sonic anemometer on CD43.

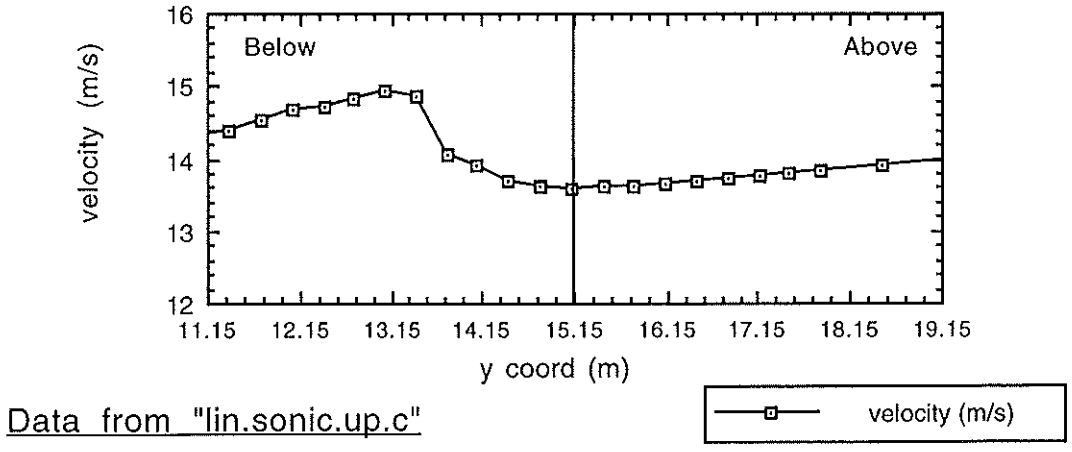

Figure 20 c) Velocity of 13.593 m/s through the Solent sonic anemometer on CD43.

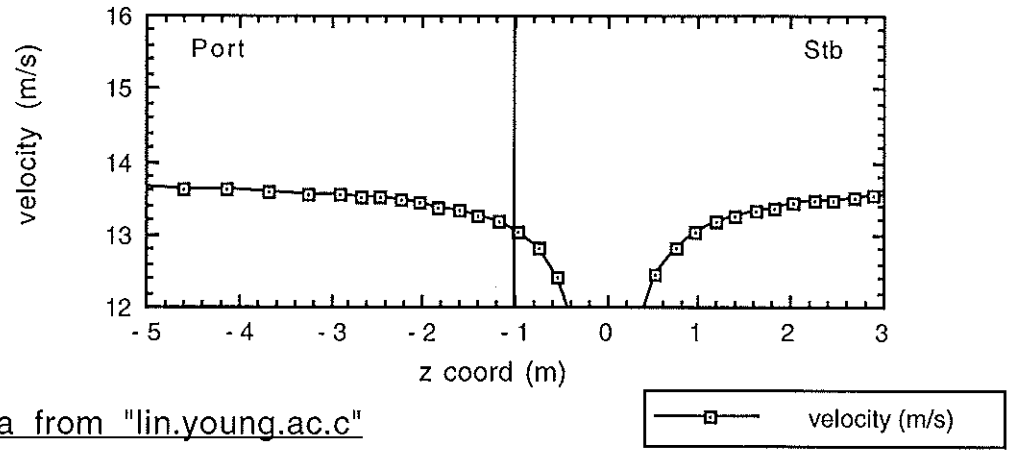

Figure 21 a) Velocity of 13.047 m/s across the Young AQ anemometer on CD43.

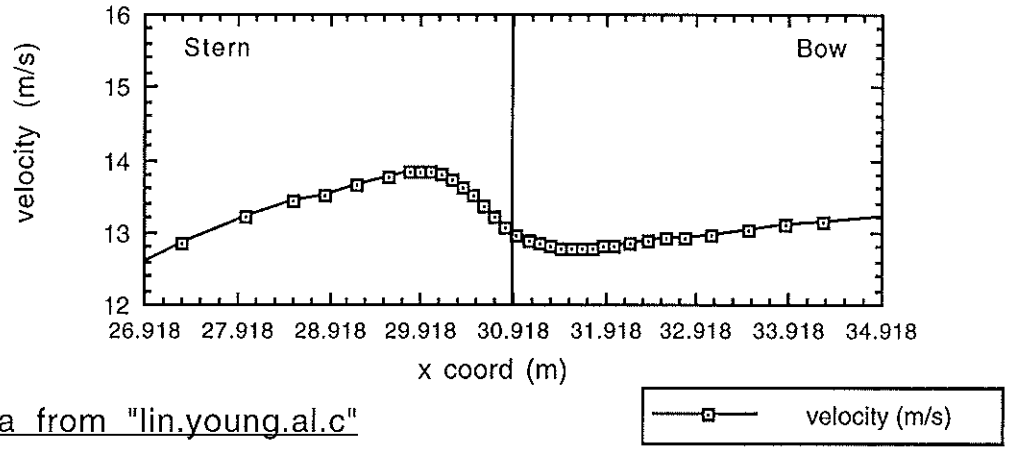

Figure 21 b) Velocity of 13.022 m/s along the Young AQ anemometer on CD43.

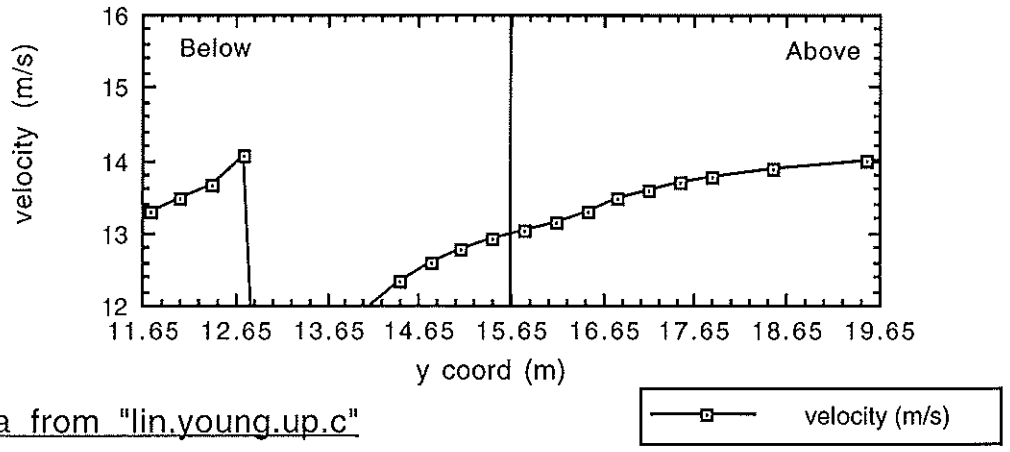

Figure 21 c) Velocity of 12.968 m/s through the Young AQ anemometer on CD43.

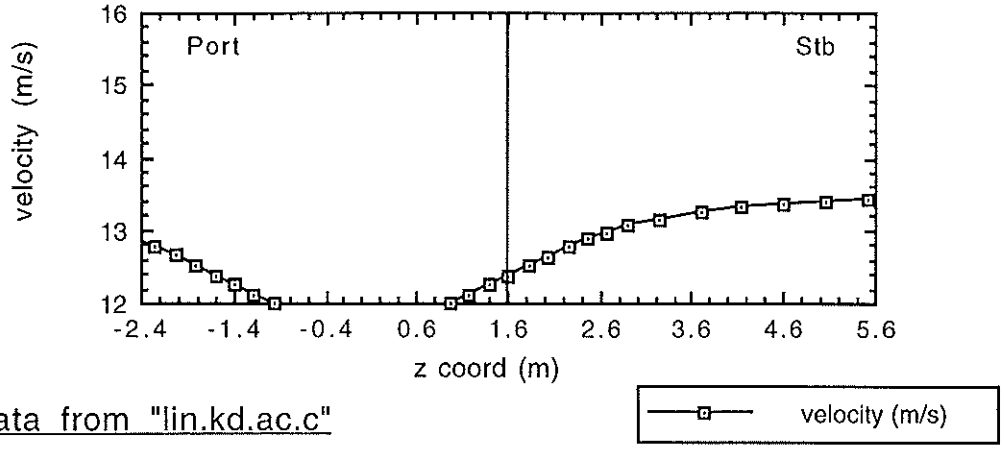

Figure 22 a) Velocity of 12.374 m/s across the Kaijo Denki anemometer on CD43.

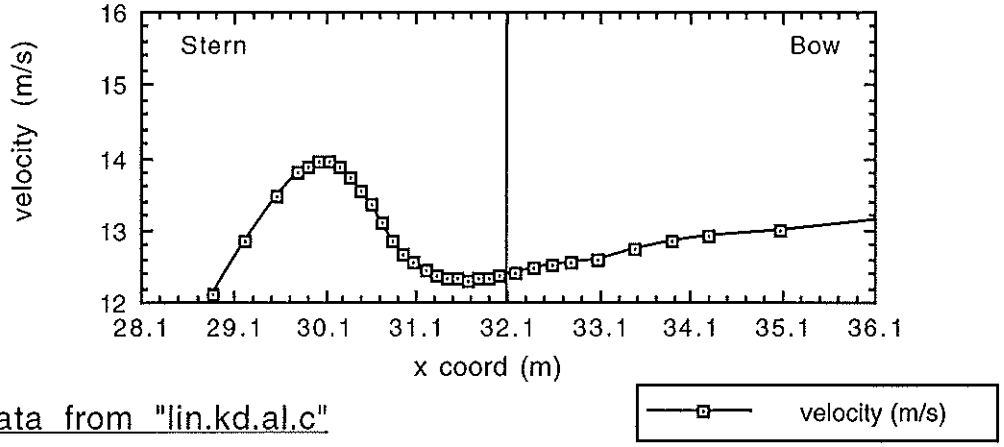

Figure 22 b) Velocity of 12.387 m/s along the Kaijo Denki anemometer on CD43.

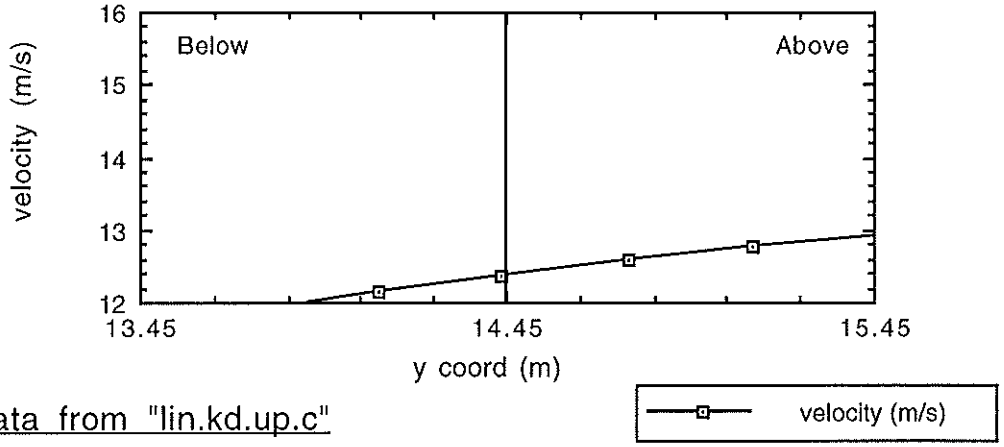

Figure 22 c) Velocity of 12.310 m/s through the Kaijo Denki anemometer on CD43.

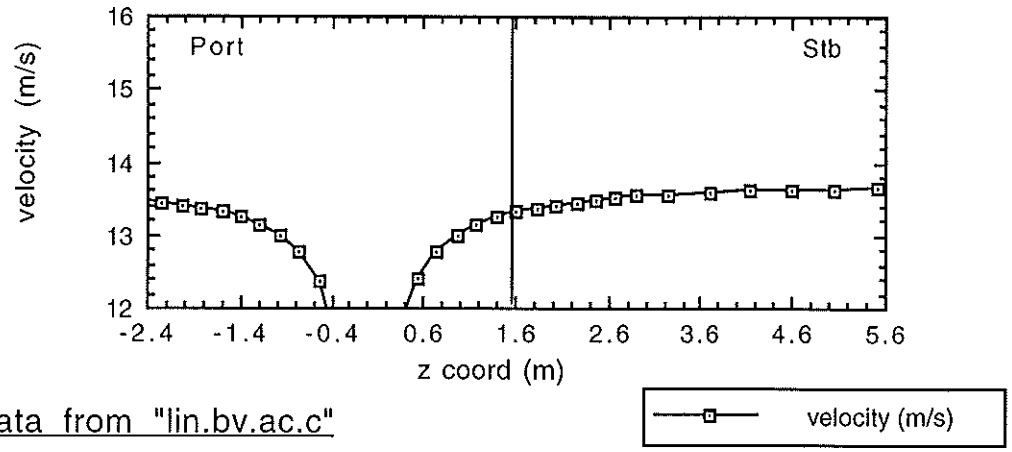

Figure 23 a) Velocity of 13.306 m/s across the Bivane anemometer on CD43.

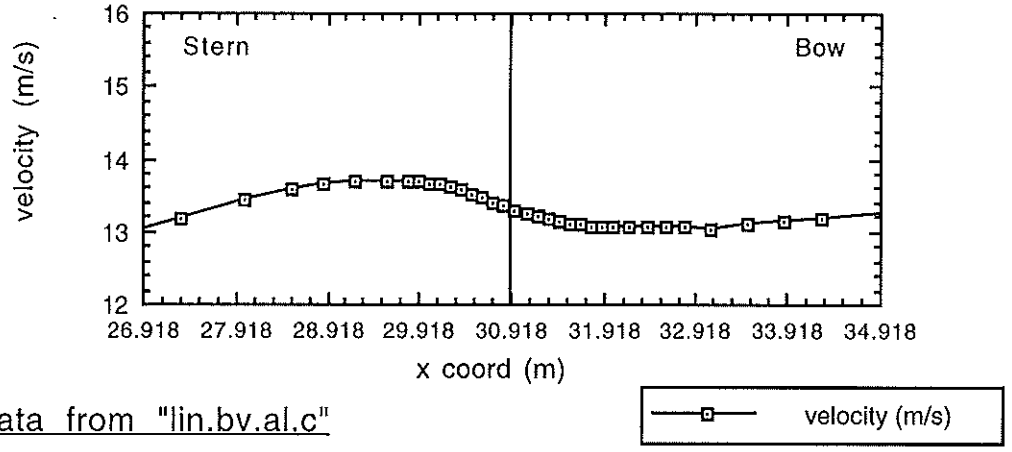

Figure 23 b) Velocity of 13.313 m/s along the Bivane anemometer on CD43.

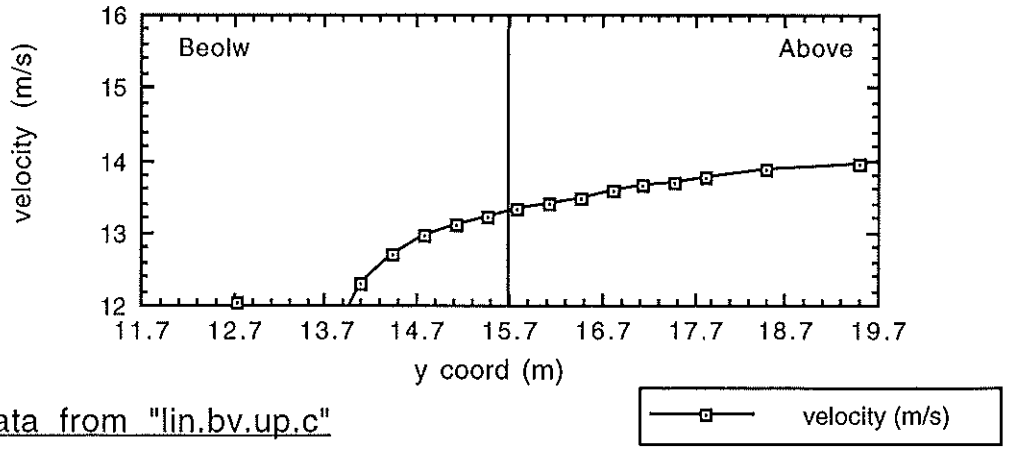

Figure 23 c) Velocity of 13.278 m/s through the Bivane anemometer on CD43.

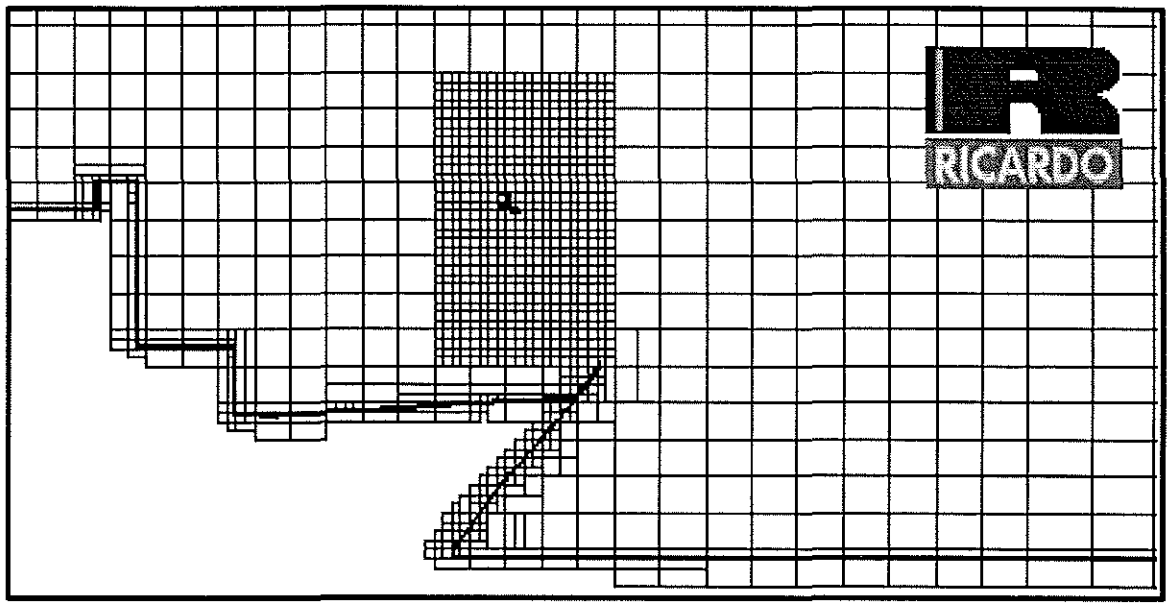

Figure 24 The mesh density on the R.R.S. Charles Darwin run 1.6/13. The mesh is viewed through the Young propeller vane anemometer site.

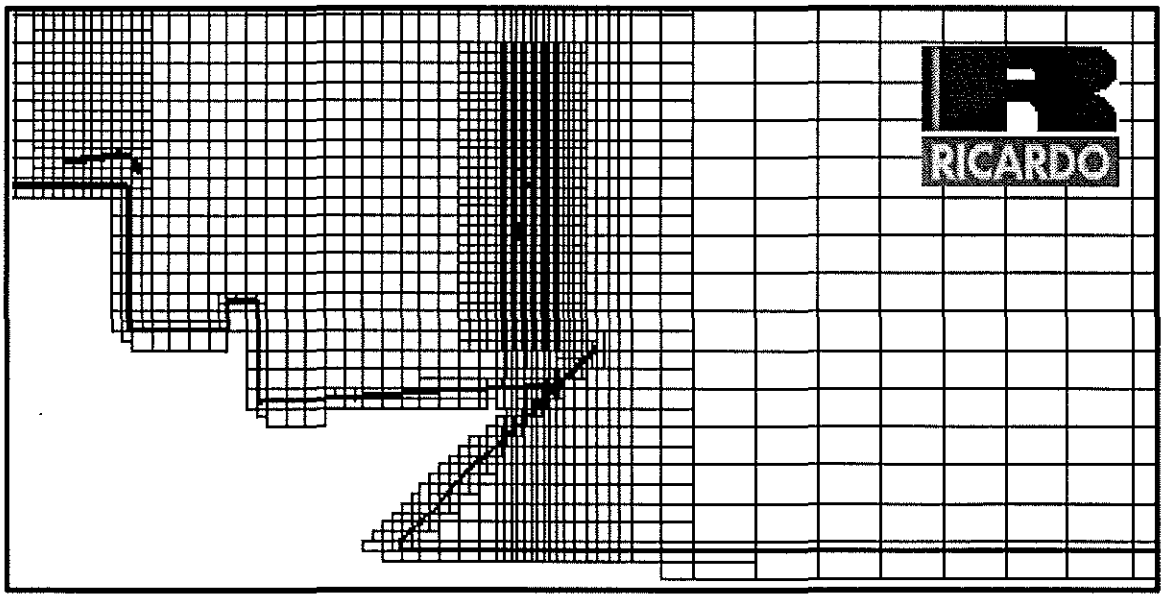

Figure 25 The mesh density on the R.R.S. Charles Darwin run 3.1/14. The mesh is viewed through the Young propeller vane anemometer site..